AD-A068 117 CLEMSON UNIV S C DEPT OF PHYSICS AND ASTRONOMY F/G 20/2
A STUDY OF CRYSTALLINE DEFECTS AND THEIR TRANSPORT IN ALKALI AZ--ETC(U)
APR 79 A L LASKAR DAHC04-75-G-0130
UNCLASSIFIED CUP-201 ARO-13059.3-P NL

1 OF 1
ADA
068117

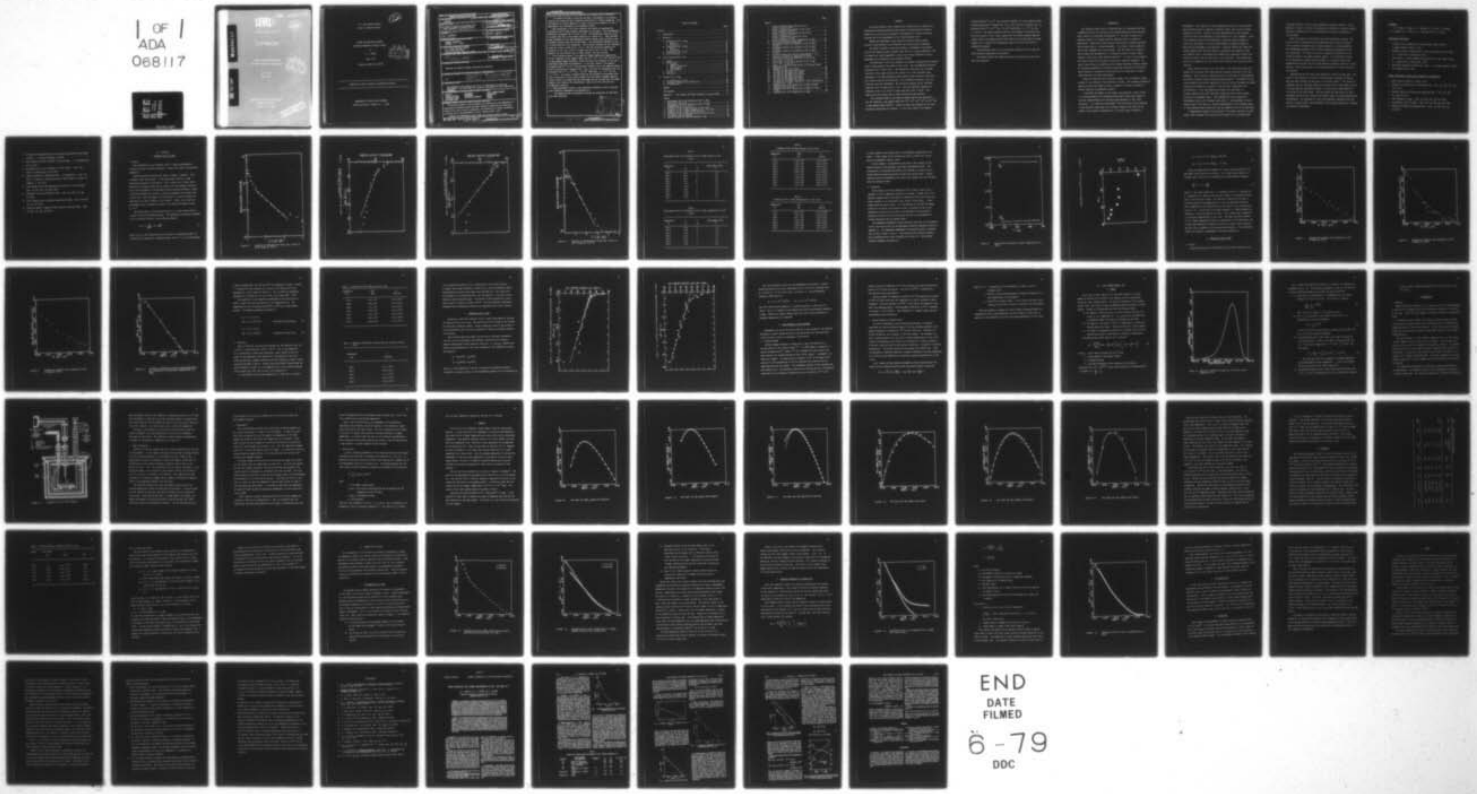

END
DATE
FILMED
6-79
DDC

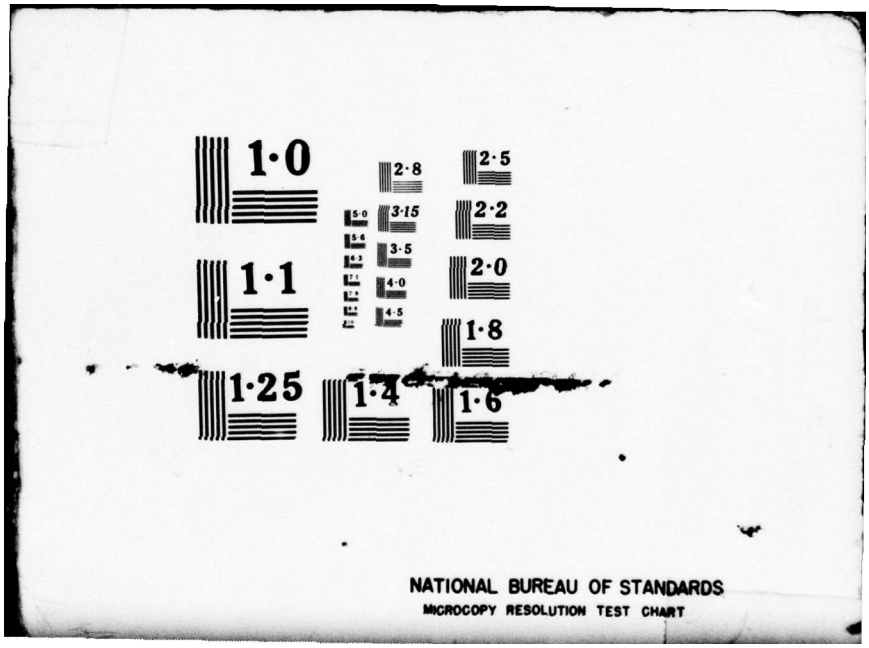
1·0
1·1
1·25
2·8
3·15
3·5
4·0
4·5
5·0
2·5
2·2
2·0
1·8
1·4
1·6
NATIONAL BUREAU OF STANDARDS
MICROCOPY RESOLUTION TEST CHART

Technical Report CUP 201

U. S. Army Research Office
Grant No. DAHC04-75-G0130

A STUDY OF CRYSTALLINE DEFECTS AND THEIR TRANSPORT IN ALKALI AZIDES

A. L. Laskar

April 1979

Department of Physics and Astronomy
Clemson University

(12)

U. S. Army Research Office

Grant No. DAHC04-75-G0130

A STUDY OF CRYSTALLINE DEFECTS AND THEIR TRANSPORT IN ALKALI AZIDES

by

A. L. LASKAR

April 1979

Technical Report No. CUP 201

Approved for Public Release; Distribution Unlimited

Department of Physics and Astronomy

Clemson University, Clemson, S. C. 29631

SECURITY CLASSIFICATION OF THIS PAGE (When Data Entered)

REPORT DOCUMENTATION PAGE

READ INSTRUCTIONS BEFORE COMPLETING FORM

1. REPORT NUMBER: ~~CUP-201~~
2. GOVT ACCESSION NO.
3. RECIPIENT'S CATALOG NUMBER: (9) rept.

4. TITLE (and Subtitle): (6) A STUDY OF CRYSTALLINE DEFECTS AND THEIR TRANSPORT IN ALKALI AZIDES.
5. TYPE OF REPORT & PERIOD COVERED: FINAL APR[illegible] 1975 - NOV[illegible]R 1978
6. PERFORMING ORG. REPORT NUMBER

7. AUTHOR(s): (10) A. L. LASKAR
8. CONTRACT OR GRANT NUMBER(s): (15) DAHC04-75-G0130

9. PERFORMING ORGANIZATION NAME AND ADDRESS: CLEMSON UNIVERSITY, CLEMSON, S. C. 29631
10. PROGRAM ELEMENT, PROJECT, TASK AREA & WORK UNIT NUMBERS

11. CONTROLLING OFFICE NAME AND ADDRESS: U. S. Army Research Office, Post Office Box 12211, Research Triangle Park, NC 27709
12. REPORT DATE: (11) APR[illegible], 1979
13. NUMBER OF PAGES: (12) 74

14. MONITORING AGENCY NAME & ADDRESS(if different from Controlling Office): (14) CUP-201
15. SECURITY CLASS. (of this report): Unclassified
15a. DECLASSIFICATION/DOWNGRADING SCHEDULE: NA

16. DISTRIBUTION STATEMENT (of this Report)

Approved for public release; distribution unlimited.

17. DISTRIBUTION STATEMENT (of the abstract entered in Block 20, if different from Report)

NA

(18) ARO (19) 13059.3-P

18. SUPPLEMENTARY NOTES

The findings in this report are not to be construed as an official Department of the Army position, unless so designated by other authorized documents.

19. KEY WORDS (Continue on reverse side if necessary and identify by block number)

DEFECTS	DIFFUSION	IONIC THERMO-CURRENT
SINGLE CRYSTALS	ANISOTROPY	RELAXATION
POTASSIUM AZIDE	ACTIVATION ENTHALPY	DOPANT
RUBIDIUM AZIDE		DIPOLE

20. ABSTRACT (Continue on reverse side if necessary and identify by block number)

Crystalline defects, their transport and interactions with impurities in potassium and rubidium azides have been studied by measuring the electrical conducitivty with ac and dc techniques, the diffusion by a tracer sectioning technique and by the measurement of ionic thermo-current (ITC).

Methods were developed to grow large and excellent quality single

DD FORM 1 JAN 73 1473 EDITION OF 1 NOV 65 IS OBSOLETE

409363

Unclassified

SECURITY CLASSIFICATION OF THIS PAGE (When Data Entered)

crystals of KN_3 and RbN_3 by the Kyropolous and solution growth techniques.

The defect structure in both KN_3 and RbN_3 is determined to be Schottky type and the charge and mass transport takes place by a vacancy mechanism. The dc conductivity studies appeared to reveal true intrinsic behavior as the ac measurements are influenced by the frequency effects.

The anisotropy in the ionic transport was studied by measuring the diffusion of $Rb^{(+)}$ in RbN_3 parallel and normal to the c-axis. The corresponding activation enthalpies are 1.43 and 1.45 eV. The diffusivity along the c-axis is higher than that in the normal direction by a factor of 3. This indicates large difference in the jump frequencies and/or entropy terms involved in the transport process along the two directions. The correlation functions in the two directions were also determined. The activation enthalpy for Ag^+ diffusion along the c-axis is found to be 1.76 eV. Thus the activation enthalpy for diffusion of Ag^+ ion (1.26 Å) is larger than that of Rb^+ (1.48 Å). This supports the size effects seen in other systems like AgCl and NaCl.

The relaxation modes of the impurity-vacancy dipoles were measured by the ITC technique in KN_3 samples doped with $Cu^{(+2)}$, $Ca^{(+2)}$, $Co^{(+2)}$, $Pb^{(+2)}$ and $Ni^{(+2)}$ and in RbN_3 samples doped with $Ba^{(2+)}$. Single ITC peaks were observed in all cases indicating single mode of relaxation. As the ionic radius of the dopants increased from Ni^{+2} to Pb^{+2}, the activation enthalpy (ξ) of the impurity-defect dipoles monotonically increased from .49 to .88 eV and the relaxation time (τ_o) decreased from 10^{-6} to 10^{-20} sec. For Ba^{2+} doped RbN_3, $\tau_o = 10^{-12}$ sec and E = 0.18 eV. The single relaxation mode and the decrease of relaxation rates with the increase of ionic radius signify that the nearest neighbor impurity vacancy dipoles are formed and that polarizability and coulomb field of larger impurity ions inhibits the orientational jumps of the host ions into the neighboring vacancies.

The preliminary results of the anisotropic diffusion of $Ag^{(+)}$ in KN_3 and anion diffusion experiments are presented.

The present project has opened up several new directions of work which have been indicated.

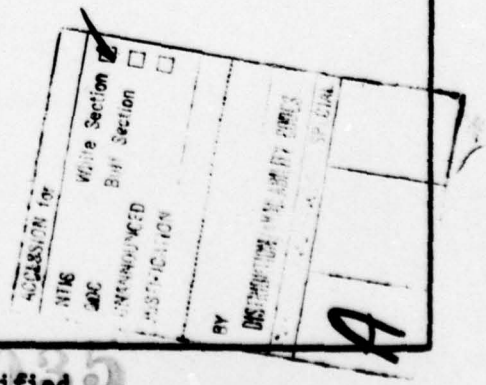

TABLE OF CONTENTS

Page

Figures

ABSTRACT

Crystalline defects, their transport and interactions with impurities in potassium and rubidium azides have been studied by measuring the electrical conductivity with ac and dc techniques, the diffusion by a tracer sectioning technique and by the measurement of ionic thermo-current (ITC).

Methods were developed to grow large and excellent quality single crystals of KN_3 and RbN_3 by the Kyropolous and solution growth techniques.

The defect structure in both KN_3 and RbN_3 is determined to be Schottky type and the charge and mass transport takes place by a vacancy mechanism. The dc conductivity studies appeared to reveal true intrinsic behavior as the ac measurements are influenced by the frequency effects.

The anisotropy in the ionic transport was studied by measuring the diffusion of Rb^+ in RbN_3 parallel and normal to the c-axis. The corresponding activation enthalpies are 1.43 and 1.45 eV. The diffusivity along the c-axis is higher than that in the normal direction by a factor of 3. This indicates large difference in the jump frequencies and/or entropy terms involved in the transport process along the two directions. The correlation functions in the two directions were also determined. The activation enthalpy for Ag^+ diffusion along the c-axis is found to be 1.76 eV. Thus the activation enthalpy for diffusion of Ag^+ ion (1.26 Å) is larger than that of Rb^+ (1.48 Å). This supports the size effects seen in other systems like AgCl and NaCl.

The relaxation modes of the impurity-vacancy dipoles were measured by the ITC technique in KN_3 samples doped with Cu^{+2}, Ca^{+2}, Co^{+2}, Pb^{+2} and Ni^{+2} and in RbN_3 samples doped with Ba^{2+}. Single ITC peaks were observed in all cases indicating single mode of relaxation. As the ionic radius of the dopants

increased from Ni^{+2} to Pb^{+2}, the activation enthalpy (ξ) of the impurity-defect dipoles monotonically increased from .49 to .88 eV and the relaxation time (τ_o) decreased from 10^{-6} to 10^{-20} sec. For Ba^{2+} doped RbN_3, $\tau_o = 10^{-12}$ sec and E = 0.68 eV. The single relaxation mode and the decrease of relaxation rates with the increase of ionic radius signify that the nearest neighbor impurity-vacancy dipoles are formed and that polarizability and coulomb field of larger impurity ions inhibits the orientational jumps of the host ions into the neighboring vacancies.

The preliminary results of the anisotropic diffusion of Ag^+ in KN_3 and anion diffusion experiments are presented.

The present project has opened up several new directions of work which have been indicated.

I. INTRODUCTION

The inorganic azides form an interesting family of compounds exhibiting a comparatively rare set of physical and chemical properties which have made them a subject of continuing investigations.[1,2] The role of azides as an energetic material is of great practical importance due to a variety of applications. Heavy metal azides (such as lead azide) are readily explodable and are widely used to initiate detonation. In contrast, alkali azides are stable ionic compounds like alkali halides. They are known to be sources of pure nitrogen when decomposition is initiated by external stimulii (photo, thermal or electrical) under suitable conditions. It is due to this property that alkali azides have long been of interest as industrial chemicals. Recently, their value as gas generators has received increased attention because the innocuous properties of the product gases make them useful for inflating safety cushions in automobiles and aircraft and as a prime mover in remote rescue operations and space applications.

Azides are chemically and structurally simple, and are potentially model systems for the theories of fast reactions in solids. The systematic progression among the azides from simple ionicity to degrees of covalency introduces a further dimension of theoretical interest.

A controlled development of the azides as gas generator (alkali azides) or as starting material for detonation (heavy metal azides) must depend on our basic understanding of the initiation and mechanism of "fast solid reactions". It is generally established[1,2] that initiation of fast reactions in such materials takes place (a) in definite region of the solid and (b) growth of this region of decomposition to a burning region followed by

deflagration. Fast reactions in these pseudostable solids are initiated when some activation energy is supplied by external stimuli which could be thermal, mechanical or optical. However, our basic understanding of these processes in terms of solid state properties of these materials is very inadequate. Solid state techniques involving the measurement of mass and charge transport in solids have contributed to our basic understanding of different systems of materials and development of new materials. Extensive studies have shown that crystal imperfections like point defects, dislocations and impurities often play dominant roles in determining the characteristic properties of many solid systems and control the rate processes in solid reactions. These factors may very well be responsible for the crucial first step for the initiation of fast reactions.

Alkali azides are known to be ionic solids. The crystalline defects are charged with the result that charge and mass transport take place by the same mechanism. Thus, electrical conductivity and the coefficient of self-diffusion are directly related through the Nernst-Einstein equation. The addition of controlled amounts of aliovalent impurities to an ionic crystal increases the defect concentration leading to an increase in both the ionic conductivity and the diffusivity. Also, the defects may interact with each other -- a divalent impurity such as Mn^{2+} may form a bound pair with a cation vacancy giving rise to permanent dipole. Both diffusion and ionic conductivity measurements can be used to monitor these effects. The measurement of ionic thermo-current (ITC) leads to a detailed understanding of the relaxation modes of these impurity-defect dipoles and thus the important roles of the impurities.

A comprehensive program for such studies of the defect structure in alkali azides, their transport and interaction with impurities was developed under

the present project. The principal experimental techniques used are: tracer diffusion of cations by serial sectioning, anion diffusion by isotopic exchange, electrical conductivity by ac and dc methods and the dipole relaxations by ITC techniques.

Many of the goals of this project have been successfully achieved. The results of these investigations have established that the defect structure in this system is Schottky type and cations migrate by a vacancy mechanism. The thermodynamic parameters for the defect formation and migration are now well established. ITC results have led to significant observations on the relaxation modes of the impurity-vacancy dipoles. Of considerable interest is the anisotropy in charge and mass transport in directions parallel and perpendicular directions due to the body-centered tetragonal structure of these crystals. Some of these results are already published as listed at the end of this section.

Reported here are the areas where significant strides have been made. The theory of ionic defects in relation to the anisotropic structures of KN_3 and RbN_3 have been developed and described in the earlier report.[3] The variety of techniques used for successful growth of excellent quality large single crystals of KN_3 and RbN_3 and experimental methods of various precise measurements are to be found in the above report. Only the results and some details of those experiments which are not covered by the earlier report and journal publications are presented. The following is a list of the personnel associated with this project at various times, the dissertations, and the papers published in journals and scientific conferences.

Personnel

D. L. Foster, K. Wagner, W. J. Mealing, B. E. Taylor, P. Cardegna, Dr. D. Hobgood, Dr. J. Weiss, Dr. J. Cook and Prof. M. G. Miller.

Dissertation and Thesis

1. A Study of Ionic Conductivity in KN_3 and RbN_3 Single Crystals -- K. Wagner (Master's Thesis, 1975).
2. Diffusion Studies of Sodium Tracer in KN_3 and Rubidium Tracer in RbN_3 -- D. L. Foster (Ph.D. dissertation, 1976).
3. Ionic Defects -- Their Transport and Interaction in AgBr, RbN_3 and KN_3 -- W. J. Mealing (Ph.D. dissertation, 1978).
4. Anisotropic Diffusion of Silver Ion in KN_3 -- P. Cardegna (Master's Thesis, to be submitted May, 1979).

Papers (Published in Journals and Presented at Conferences)

1. ARO-D Technical Report No. CUP101 (1975)
2. Diffusion of Sodium Tracer in Potassium Azide -- Bull. Am. Phys. Soc. 19, 1105 (1974)
3. Schottky Defects in Potassium and Rubidium Azides -- Bull. Am. Phys. Soc. 19, 372 (1974)
4. Ionic Transport in RbN_3 -- Bull. Am. Phys. Soc. 20, 470 (1975)
5. The Diffusion of Rb^* in RbN_3 -- Bull. Am. Phys. Soc. 21, 322 (1976)
6. Conductivity Studies of Rubidium Azide -- Bull. Am. Phys. Soc. 21, 322 (1976)

7. The Growth and Characterization of Potassium and Rubidium Azide Single Crystals -- J. Crystal Growth 32, 33 (1976)

8. Ionic Defects and Their Transport in KN_3 and RbN_3 -- J. de Physique 37, C7-471 (1976).

9. Anisotropy in the Ionic Transport in Alkali Azides -- Proc. 19th Colloq. de Metallurgie 1, 829 (1976)

10. Impurity Diffusion in Potassium Azide -- A Pseudohalide -- Proc. Int. Conf. on "Defects in Insulating Crystals" CONF-771002, U.S. Dept. of Commerce, p. 132 (1977)

11. Ionic Thermo-current and Spontaneous Polarization in KN_3 and RbN_3 -- Bull. Am. Phys. Soc. 22, 1256 (1978)

12. Diffusion of Silver in Rubidium Azide -- Bull. Am. Phys. Soc. 24, 99 (1979)

13. Ionic Thermo-current in Impurity-doped KN_3 and RbN_3 -- Bull. Am. Phys. Soc. 24, 99 (1979)

14. Relaxation Modes of Impurity-Vacancy Dipoles in KN_3 and RbN_3 -- Bull. Am. Phys. Soc. 24, 378 (1979).

II. DIFFUSION

A. Diffusion of Rb^+ in RbN_3

1. Results

The investigation of the diffusion of Rb^+ is RbN_3 was performed by a tracer and serial sectioning technique.[3] Some of the results are published (Appendix-1).

Typical penetration profiles are shown in Figures 1 through 4. They, in general, show three regions. In the upper region there is a large scattering and upturn in these points. This is partly due to extra tracer material on the surface which did not dissolve into the specimen, and partly due to the misalignment of the specimen during microtome-sectioning. Though a exacting procedure was followed to align the specimens with 25 meter long optical lever, some misalignment still persisted as 1 μm thin sections were taken due to the small diffusity of the cations. Tables 1 and 2 show the misalignment errors estimated according to the equation developed by Shirn et. al.[4]

The middle region in the penetration plots is a linear section which is a result of the bulk diffusion process. The experimental conditions correspond to the "thin-film" solution of the diffusion equation:

$$C(x,t) = \frac{C_o}{2\sqrt{\pi Dt}} \exp\left(\frac{-x^2}{4Dt}\right) \qquad (1)$$

where, $C(x,t)$ is the concentration of the tracer at a penetration depth "x" from the active surface for a diffusion anneal time "t", C_o is the total amount

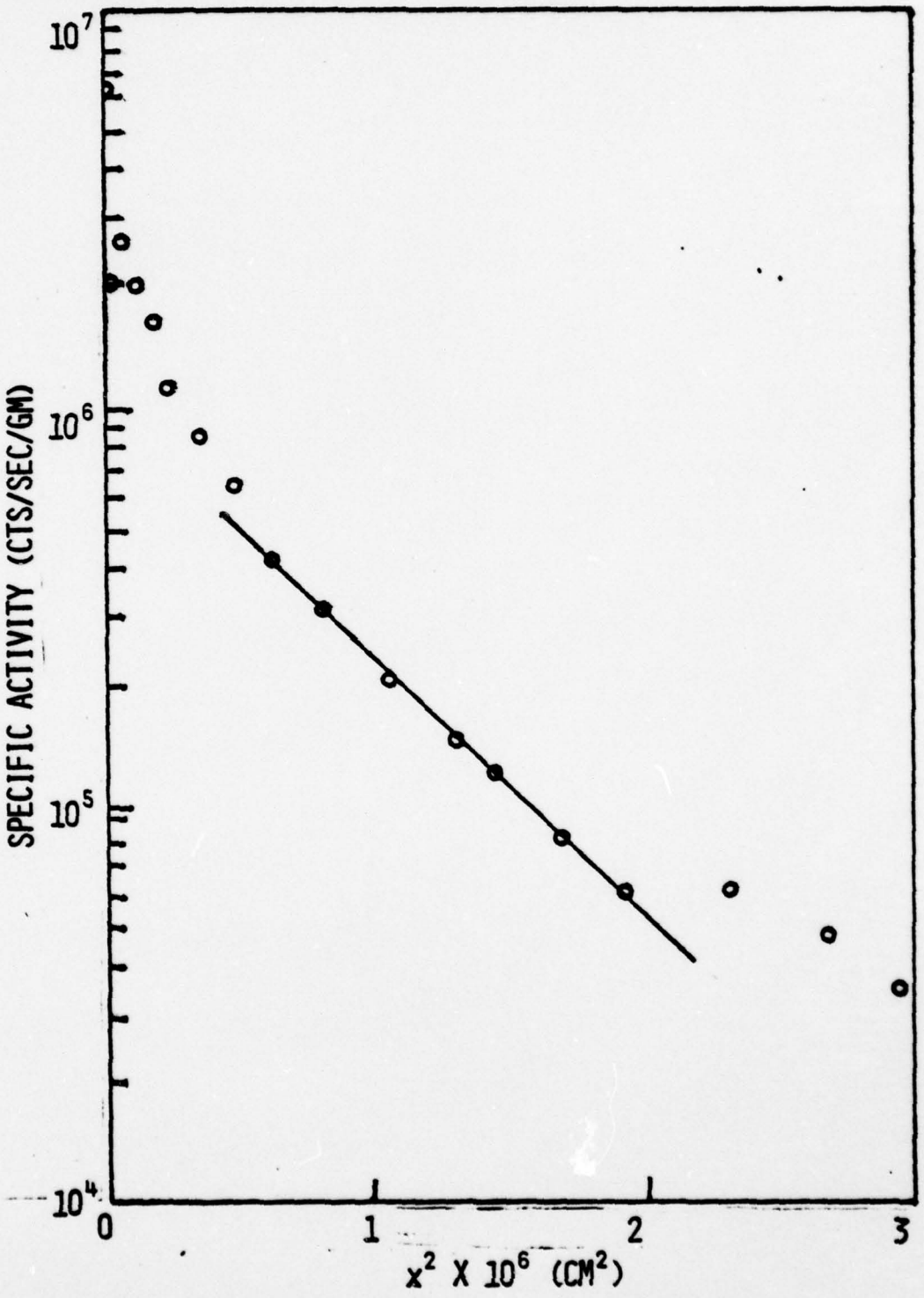

Figure 1. Profile of Penetration Along the c-axis of Rb^* in RbN_3 at 240°C.

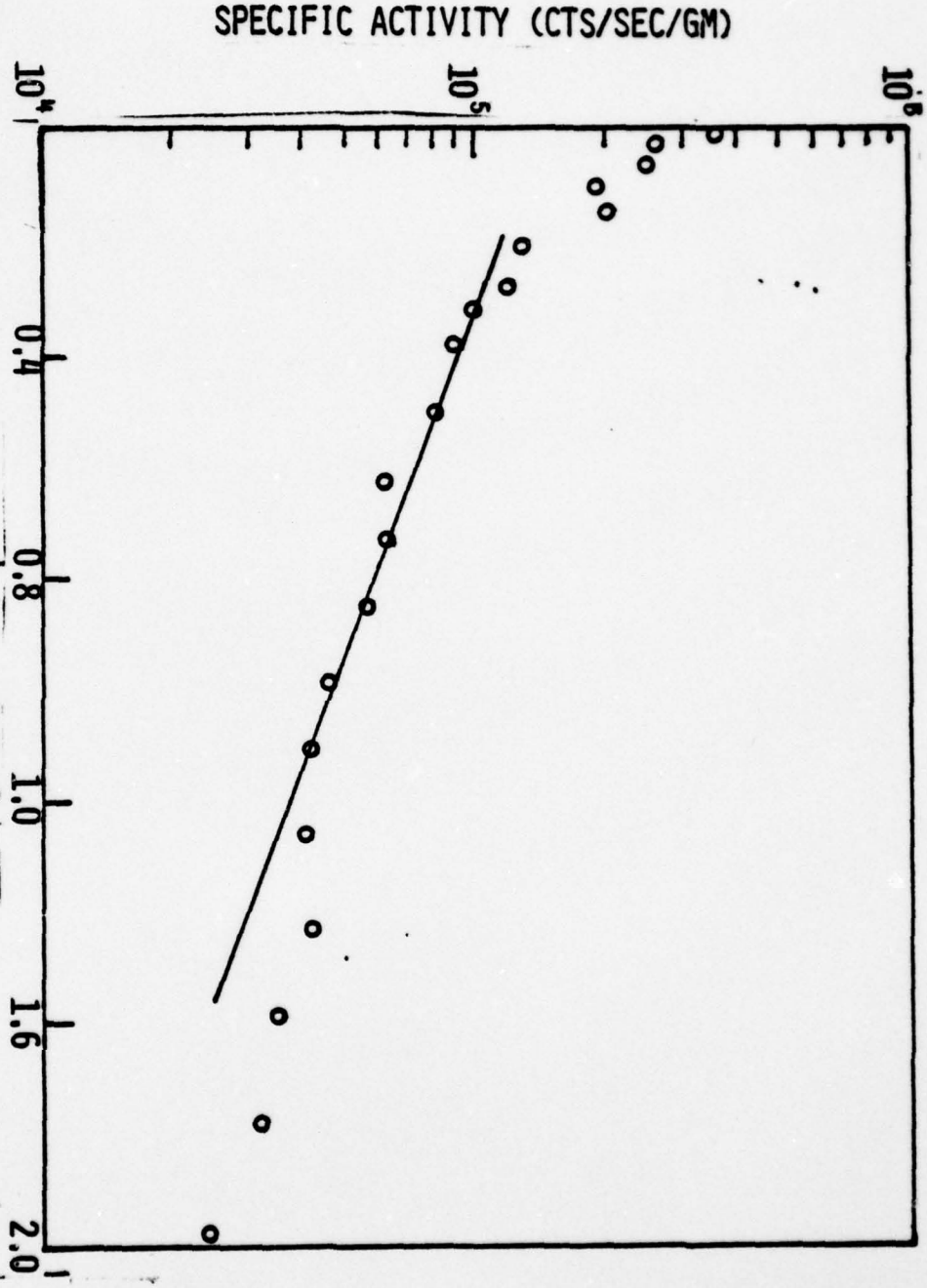

Figure 2. Profile of Penetration Normal to the c-axis of Rb^+ in RbN_3 at 249.8°C

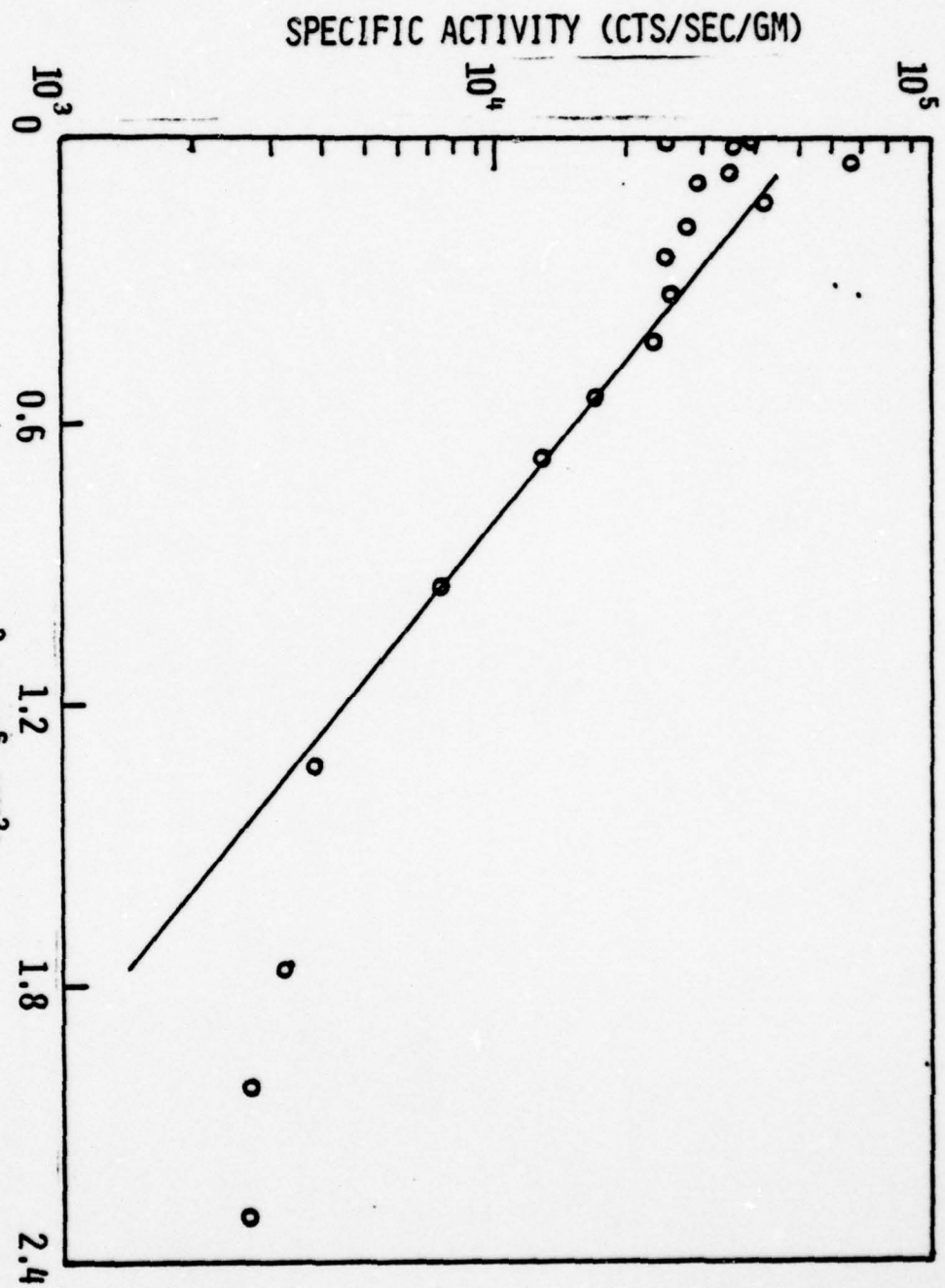

Figure 3. Profile of Penetration Normal to the c-axis of Rb in RbN_3 at 270.7°C

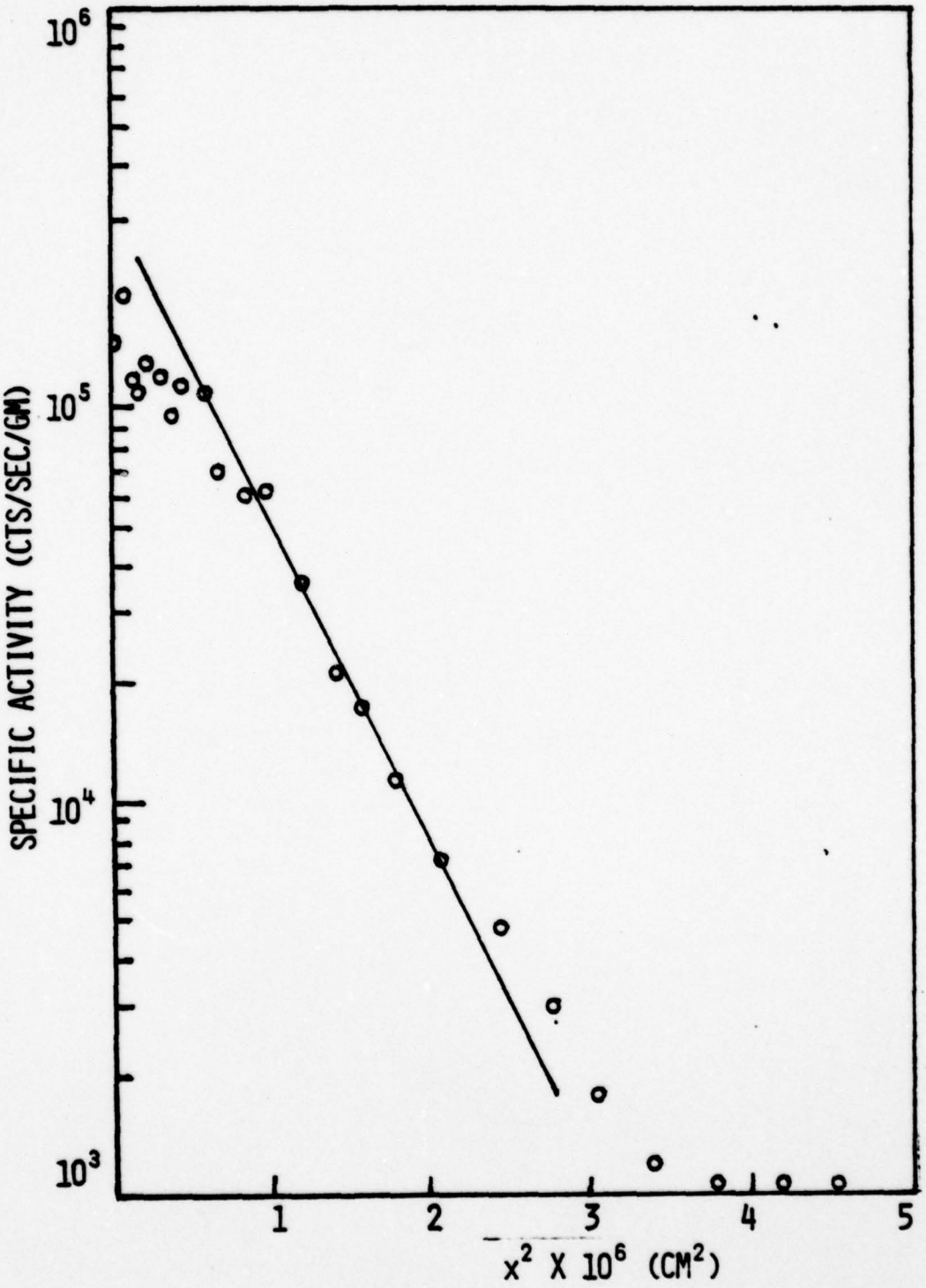

Figure 4. Profile of Penetration Along the c-axis of Rb^* in RbN_3 at 244.9°C

Table 1

Misalignment Error for Diffusion of Rb* in RbN_3 Parallel to the c-axis

Temperature °C	ρ μm	s μm	Misalignment Error %
276.5	12.2	4	1.8
266.5	10.6	3	1.3
255.7	10.9	7	6.9
249.2	23.7	13	5.0
244.9	8.74	3	2.0
240.3	8.14	1	0.3
232.1	13.9	3	0.8
228.7	16.9	8	3.7
224.3	8.80	3	1.9
216.2	13.2	7	4.7

Table 2

Misalignment Error for Diffusion of Rb* in RbN_3 Perpendicular to the c-axis

Temperature °C	ρ μm	s μm	Misalignment Error %
274.2	8.24	3	2.2
270.7	7.12	2	1.3
264.2	6.57	3	3.5
255.7	6.12	1	0.4
249.8	9.16	2	1.2
240.3	5.22	2	2.4
224.2	7.84	4	6.4

Table 3

Diffusion of Rb* in RbN_3 Parallel to the c-axis

Temperature °C	Time Sec	D cm^2/sec
276.5	5.19×10^4	7.23×10^{-12}
266.5	7.34×10^4	3.88×10^{-12}
255.7	9.04×10^4	3.29×10^{-12}
249.2	8.15×10^5	1.77×10^{-12}
244.9	6.08×10^5	3.14×10^{-13}
240.3	1.71×10^5	9.72×10^{-13}
232.1	7.69×10^5	6.36×10^{-13}
228.7	2.12×10^6	3.38×10^{-13}
224.3	6.33×10^5	3.07×10^{-13}
216.2	2.13×10^6	2.05×10^{-13}

Table 4

Diffusion of Rb* in RbN_3 Perpendicular to the c-axis

Temperature °C	Time Sec	D cm^2/sec
274.2	8.02×10^4	2.12×10^{-12}
270.7	5.87×10^4	2.16×10^{-12}
264.2	8.77×10^4	1.23×10^{-12}
255.7	9.04×10^4	1.04×10^{-12}
249.8	3.48×10^5	6.04×10^{-13}
240.3	3.46×10^5	1.98×10^{-13}
224.2	1.21×10^6	1.27×10^{-13}

of tracer placed on the surface and D is the diffusion coefficient of the tracer. A least square fit of the data was used to extract the D values. These are displayed in Tables 3 and 4.

For most samples, the penetration plots have a third region (in the deeper sections of the specimens) which show considerable scatter. The trailing-off of the penetration profiles are believed to be due to the enhanced diffusion along dislocations or other shor-circuit paths. Surface diffusion had been eliminated as the sides of the samples were well polished after the diffusion anneal.

2. *Discussion*

The anistropy of the self diffusion of Rb^+ in RbN_3 is seen in Fig. 5 (Appendix I) and is adequately discussed in the paper. Indeed, this is an important demonstration of the effect of correlation factor on the mass and charge transport in an anisotropic ionic crystal, such as RbN_3 -- a rare example among the ionic solids. It is interesting to note that the higher diffusivity of the Rb^+ ions along the c-axis in contrast to that in the perpendicular direction is not due to the difference of the activation enthalpies of motion in the two directions but due to the difference of attempt frequencies and the entropy values.

The temperature dependence of the correlation functions in an anisotropic crystal can cause an error in the determined activation enthalpies form Fig. 5 (Appendix 1). The temperature dependence of correlation factors, estimated from our data is seen in Fig. 5. The correction for activation enthalpy may be determined from a plot of $\log[D^*(T)/f]$ versus $1/T$. The modified diffusion parameters obtained are:

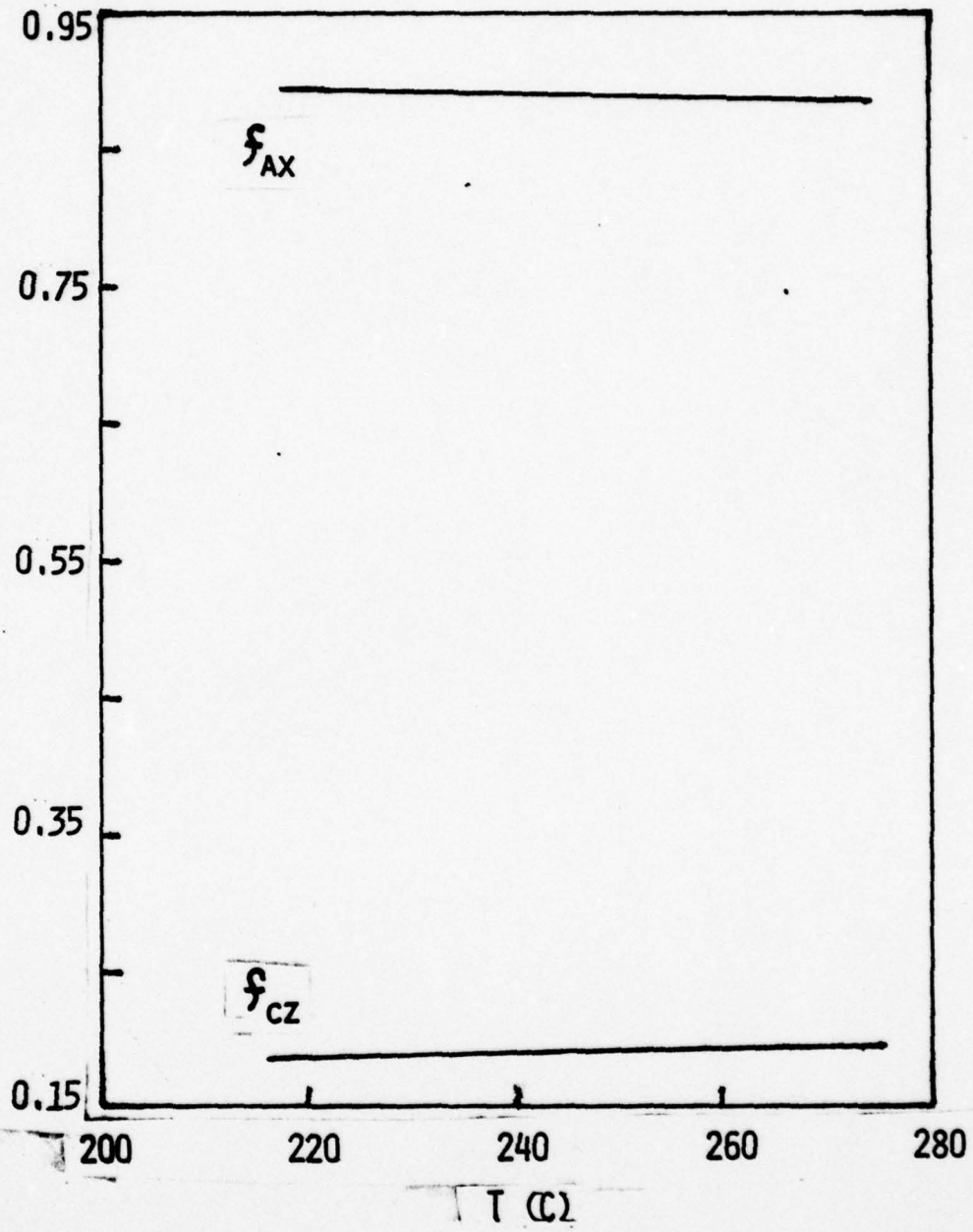

Figure 5. Correlation Functions Versus Temperature for RbN_3

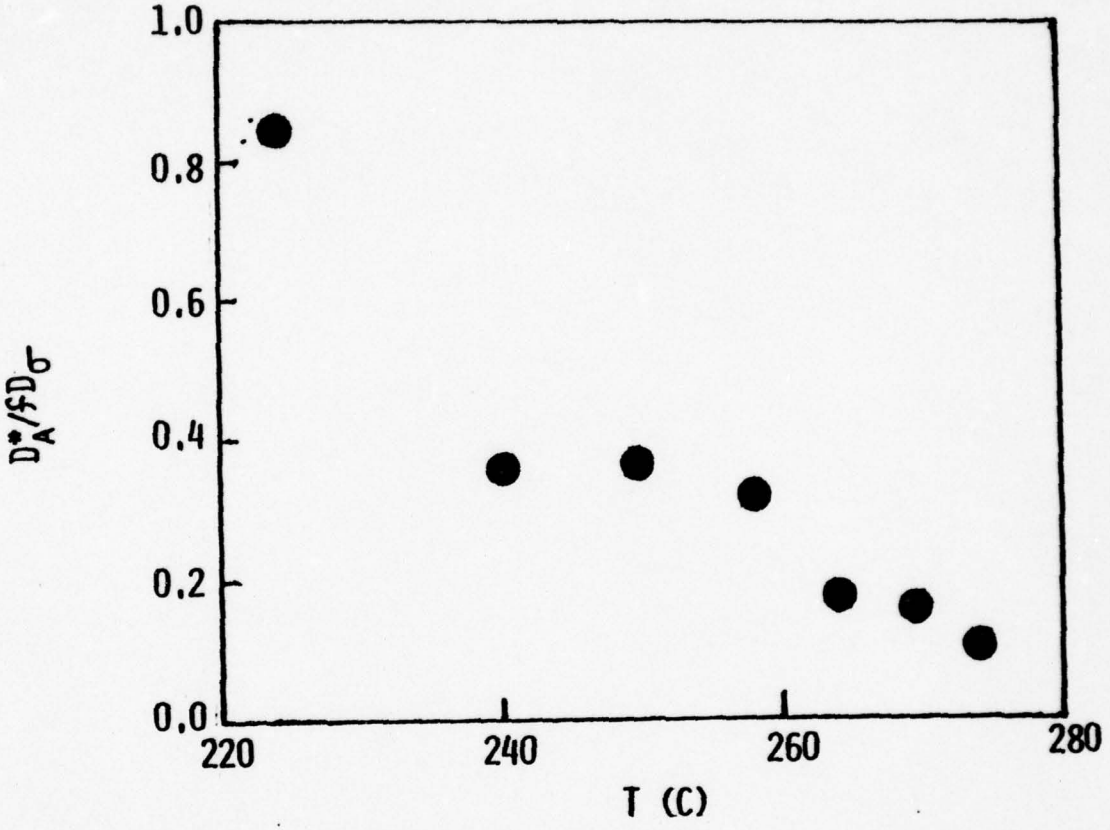

Figure 6. Plot of D_a/D_σ Versus Temperature

$$H_c = 1.41 \pm 0.07 \text{ eV}, \quad D_o^c/f_{BZ} = 295 \text{ cm}^2/\text{s}$$

$$H_a = 1.45 \pm 0.13 \text{ eV}, \quad D_o^a/f_{AX} = 61 \text{ cm}^2/\text{s} \qquad (2)$$

Since the charge and mass transport in a ionic solid take place by the same defect species they are correlated. For a single mobile species in a isotropic ionic crystal this is governed by the Nernst-Einstein equation:

$$\frac{D^*}{D_\sigma} = f \ , \quad D_\sigma = \frac{KT\sigma}{e^2 N} \qquad (3)$$

where D^* = the tracer diffusivity, f = correlation factor, σ = conductivity, T = temperature, N = number of ions per unit volume, K is boltzman constant, and e is the electronic charge. The electrical conductivity for RbN_3 in directions parallel and perpendicular to c-axis as reported[3] already can now be compared with the diffusivities of the cations in the two directions using eq. (3). As discussed in the paper (Appendix 1), a good agreement was obtained in a direction parallel to c-axis. Fig. 6 shows such a comparison in a direction perpendicular to the c-axis. The rapid turn down of points D^*/D_σ at higher temperatures indicate a contribution to the conductivity due to some other mechanism in addition to that due to single cation vacancies. The most likely candidates are the anions and divacancies. This speculation needs to be tested by a measurement of the anion diffusivity.

B. Diffusion of Ag^+ in RbN_3

1. Results

Penetration profiles for the diffusion of Ag^* tracer along the c-axis

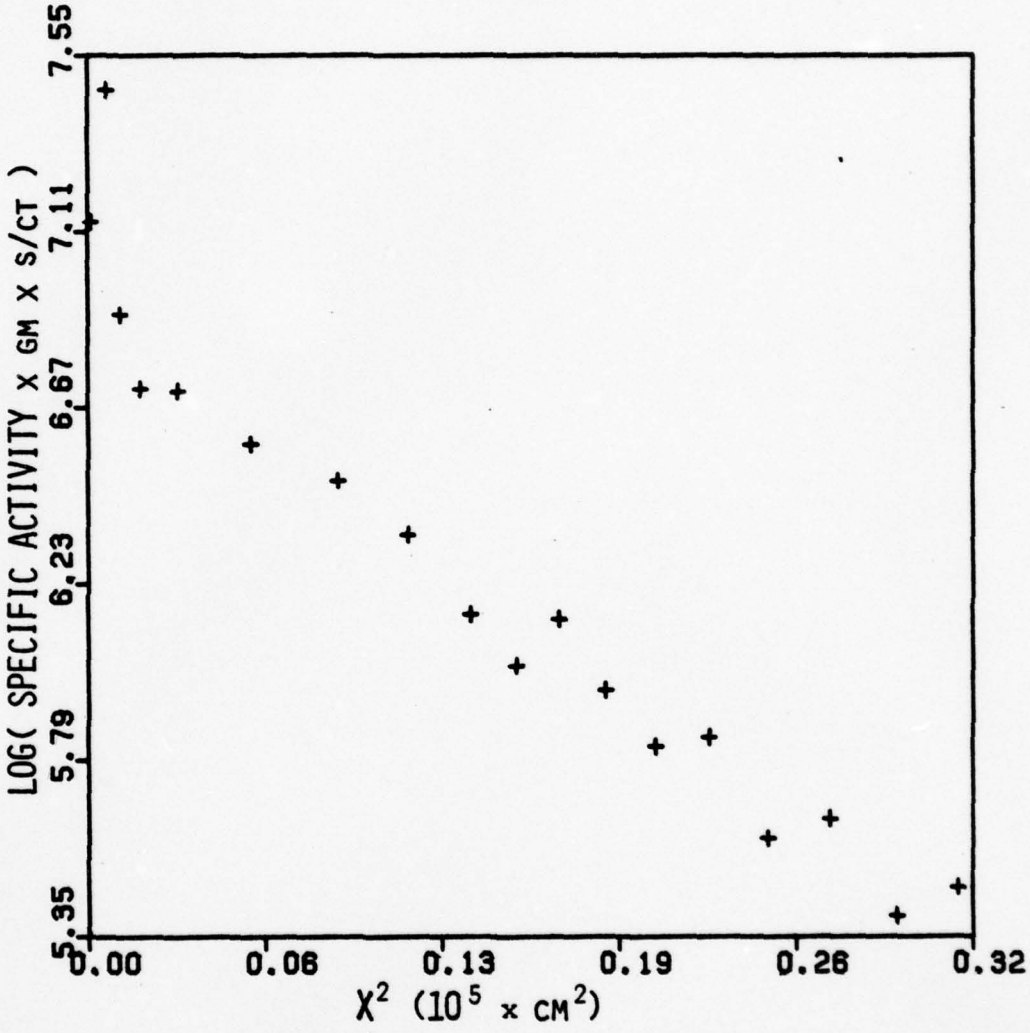

Figure 7. Penetration Profile for Diffusion of Ag^* in RbN_3 at 220°C.

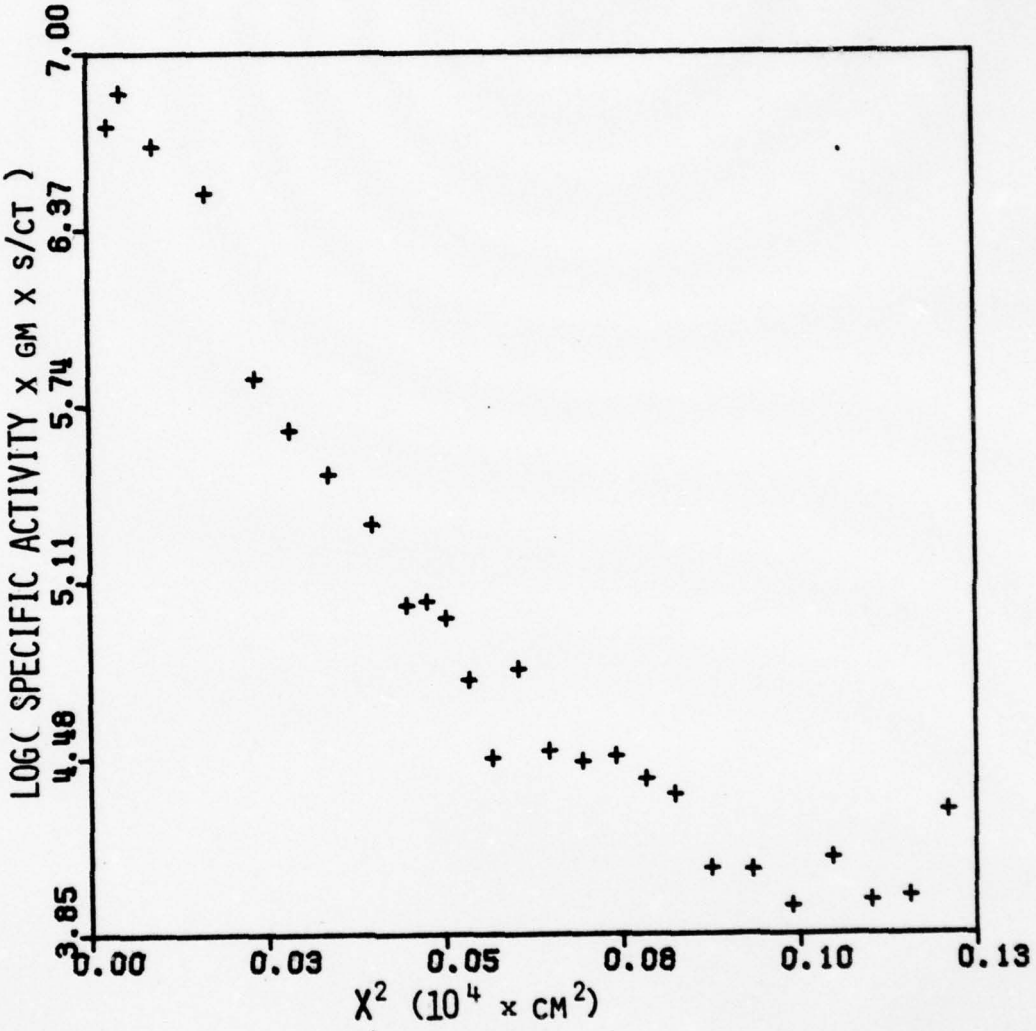

Figure 8. Penetration Profile for Diffusion of Ag^* in RbN_3 at 269°C.

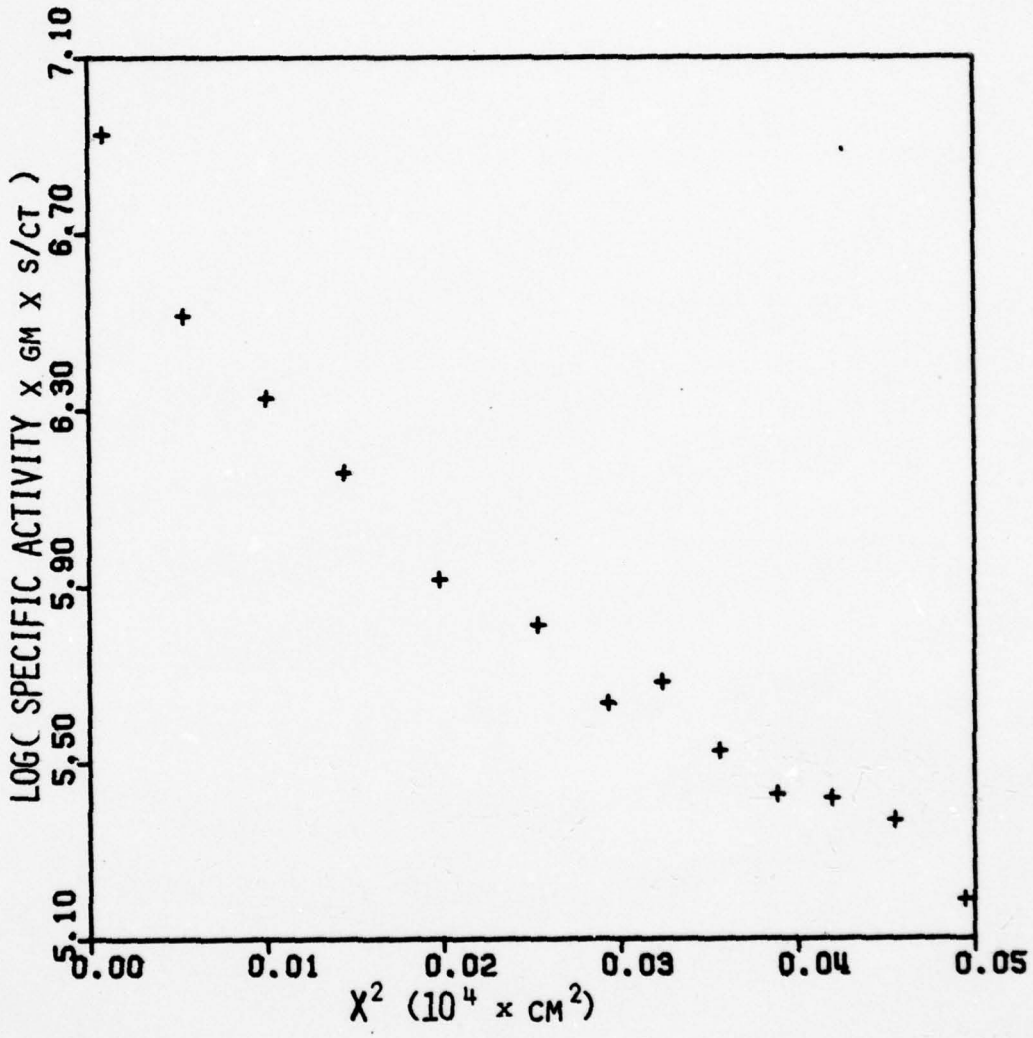

Figure 9. Penetration Profile for Diffusion of Ag^* in RbN_3 at 275°C.

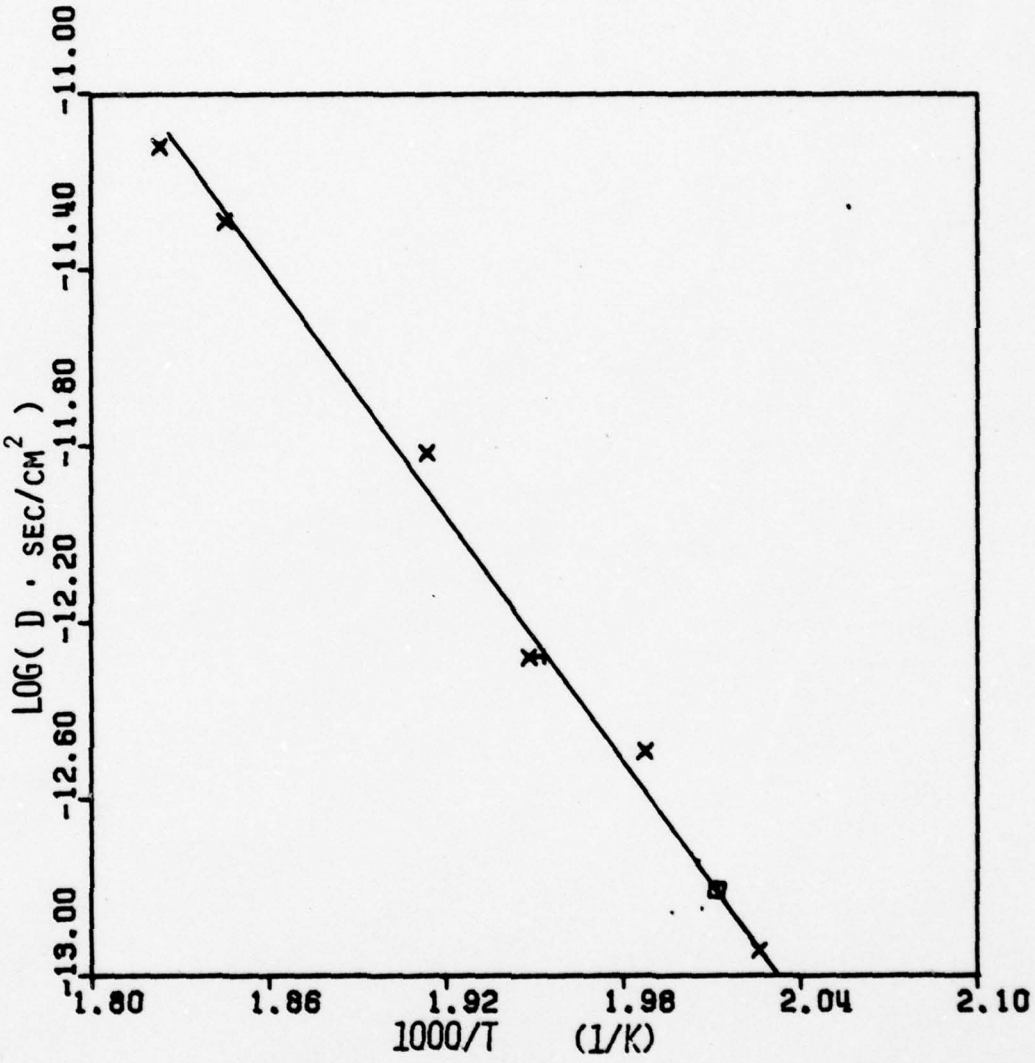

Figure 10. Diffusion Coefficient Plotted Logarithmically as a Function of Reciprocal Temperature for RbN_3.

in RbN_3 at temperatures 220, 269 and 275°C are displayed in Figures 7 through 9. Following the same rationale as in section A the diffusivities were determined by a least square fit (Table 5). Fig. 10 shows the temperature dependence of the diffusivity of Ag^+ in RbN_3 in the range 220°C - 275°C.

The uncertainty in the temperature measurement for the data point at 240°C is shown by an error bar parallel to the temperature axis. The temperature for this run drifted from 236°C to 240°C due to some unknown artifact. The diffusion parameters obtained are

$$H_c = 1.76 \pm 0.07 \text{ eV}$$
$$D_o^c = 1.14 \times 10^5 \text{ cm}^2/\text{s} \qquad \text{(excluding 240 data point)} \qquad (4)$$

$$H_c = 1.77 \pm 0.08 \text{ eV}$$
$$D_o^c = 1.50 \times 10^5 \text{ cm}^2/\text{s} \qquad \text{(including 240 data point)} \qquad (5)$$

2. Discussion

Thus, we find that the activation enthalpy for the diffusion of Ag^+ ion (1.26 Å) is larger than that of Rb^+ (1.48 Å). This is not unexpected. It is interesting to observe that Fredericks' recent review[5] of the size effect of the monovalent cation impurities in the monovalent lattice of alkali halides show a general trend that ions with smaller size need a larger activation enthalpy of motion. Recently Batra and Slifkin[6] reported that H_m for Na^+ diffusion in AgCl is 0.5 eV compared to 0.3 eV for vacancy diffusion of Ag^+ though ionic radii are 0.97 and 1.26 Å respectively.

As noted before the consistent appearance of a long "tail" or plateau

Table 5. Diffusion of Ag* in RbN_3 Along the C-Axis

Temperature (°C)	Time (Sec)	D (cm^2/sec)
275.5	5.13×10^4	7.58×10^{-12}
268.9	6.39×10^4	5.12×10^{-12}
249.6	1.73×10^5	1.53×10^{-12}
240.3	4.29×10^5	5.28×10^{-13}
230.2	6.77×10^5	3.22×10^{-13}
224.6	9.62×10^5	1.56×10^{-13}
220.6	2.08×10^6	1.14×10^{-13}

Table 6. Diffusion Coefficients of Ag* in RbN_3 for the Short Circuit Paths

Temperature (°C)	D (cm^2/sec)
268.9	2.14×10^{-11}
249.6	9.85×10^{-12}
245.3	2.1×10^{-12}
240.3	1.23×10^{-12}
230.2	7.50×10^{-13}

in the penetration profile is not a characteristic of the bulk diffusion. It appears that surface diffusion is ruled out as, after the diffusion anneal, enough material from the side surfaces were polished off. This leaves only one candidate as a contributing factor for this behavior -- the short circuit diffusion along dislocation pipes. The density of the dislocations in the as grown crystals is found to be about $10^6/cm^2$. The pipe diffusion coefficients estimated from the penetration profiles are approximate and listed in Table 6.

C. Diffusion of Ag^+ in KN_3

Anisotropy in the ionic transport in KN_3 is being investigated by studying the diffusion of Ag^+ ion in KN_3. The short half-life K^* isotope is not suitable for such tracer diffusion studies. Being a homovalent cation in KN_3 crystal, a low concentration of Ag^+ ions are not expected to affect the intrinsic behavior of the system.

Since the melt-grown KN_3 single crystals grow in different orientations with the c-axis, two specimens with different orientations are diffusion annealed simultaneously under identical conditions. D_{zz} and D_{xx}, diffusivities parallel and perpendicular to the c-axis respectively, are obtained by solving the equations:

$$D_1 = D_{xx}\sin^2\theta_1 + D_{zz}\cos^2\theta_1$$

$$D_2 = D_{xx}\sin^2\theta_2 + D_{zz}\cos^2\theta_2$$

where D_1 is the diffusivity of Ag^+ for a specimen with diffusion direction oriented at an angle θ_1 and D_2 is the corresponding quantity for an orientation θ_2.

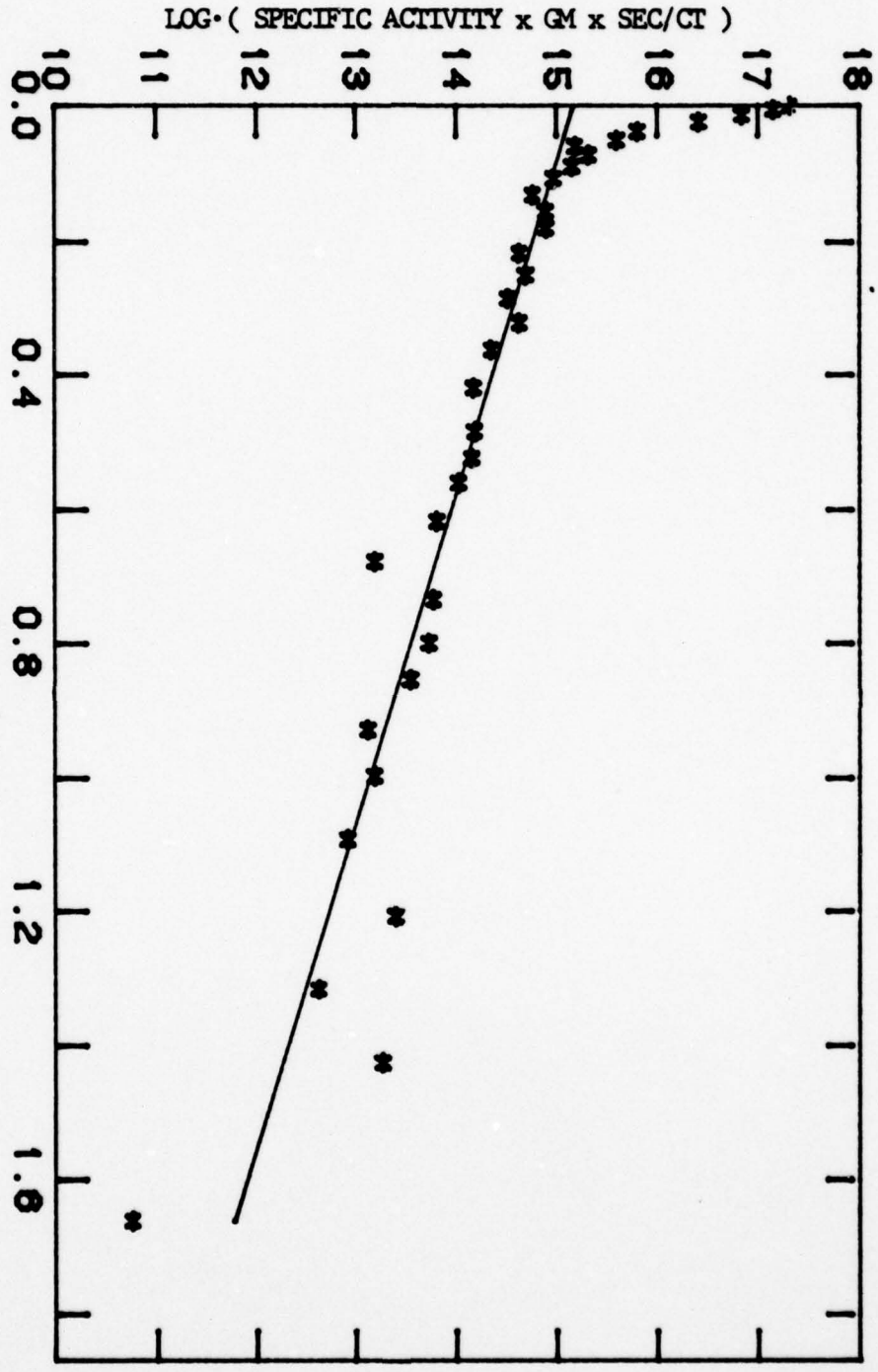

Figure 11. Penetration Profile for Diffusion of Ag^* in KN_3; for $\theta = 68^o$, $T = 257.6^oC$.

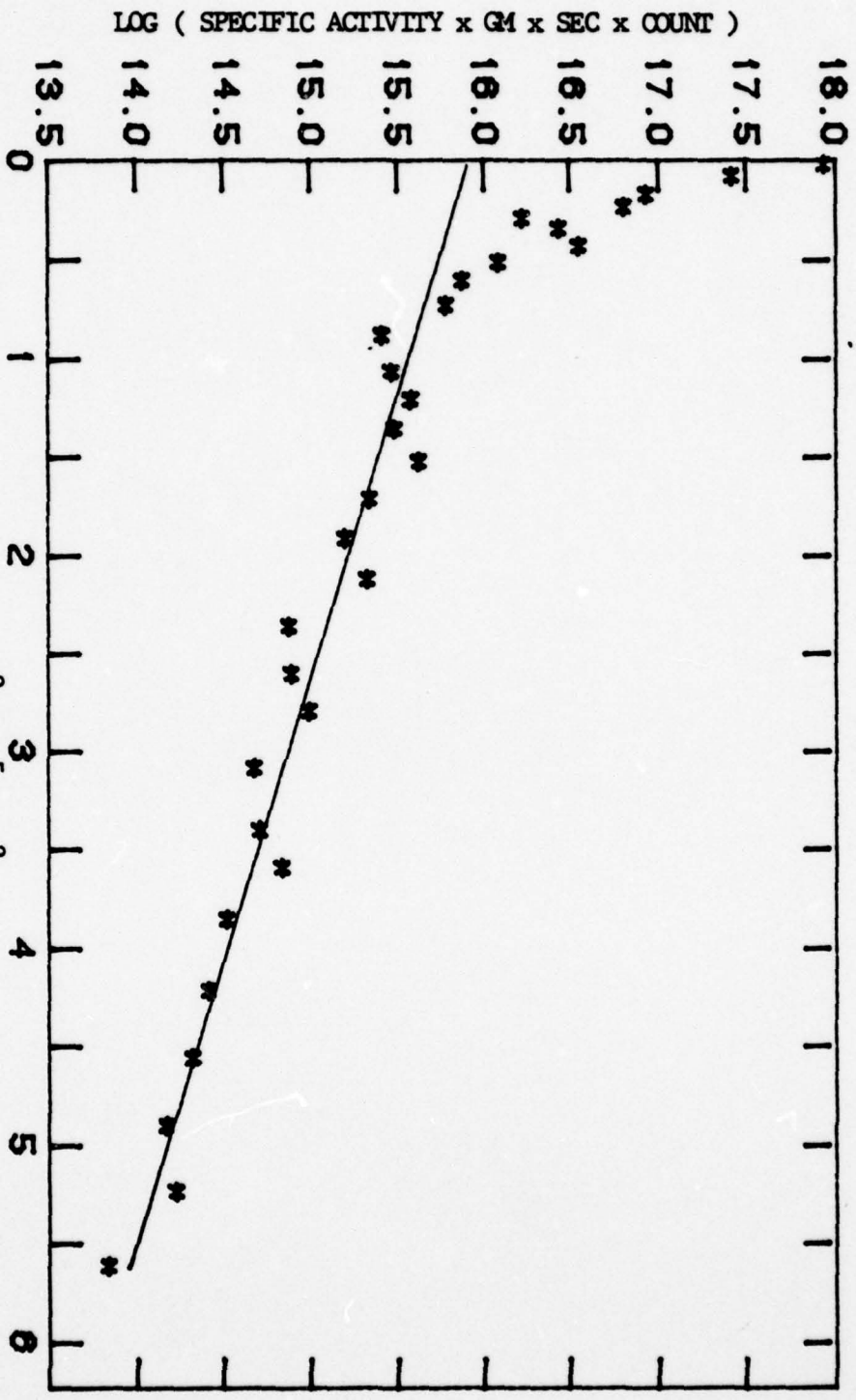

Figure 12. Penetration Profile for Diffusion of Ag^* in KN_3 for $\theta = 77^o$, $T = 257^oC$.

Only the preliminary results of some experiments are available. Typical penetration profiles for such a simultaneous run at 257.6°C for specimens with $\theta_1 = 68^\circ$ and $\theta_2 = 77^\circ$ are seen in Fig. 11 and Fig. 12. The corresponding diffusion coefficients are

$$D_1 = 1.6 \times 10^{-12} \text{ cm}^2/\text{sec}, \qquad D_2 = 2.8 \times 10^{-12} \text{ cm}^2/\text{sec}$$

This will indicate that diffusion in a direction parallel to the c-axis is slower. This is in contrast to the observations about the anisotropic diffusion in RbN_3. However any further comment should wait until these experiments at different temperatures are completed.

D. Anion Diffusion in KN_3 and RbN_3

Experimental set-up for the anion diffusion in KN_3 and RbN_3 by two different techniques is almost completed and only some exploratory runs have been made. A brief outline of these two techniques is given below.

1. Isotope Exchange

Isotope exchange technique is being used to study the diffusivity of nitrogen which has only stable isotope N^{15}. If a KN_3^{13} sample is annealed in a capsule enriched with N^{15} isotope, N^{15} will exchange with azide radicals and these radicals will diffuse through the bulk of the crystals. Consequently two things will happen: (1) there will be a depletion of N^{15} in the capsule with time and (2) the concentration of N^{15} will decrease with distance into the sample measured from the surface. This phenomenon depends on both exchange rate and diffusion rate. But diffusion being the rate limiting process, the diffusion coefficient can be estimated by measuring the total depletion of N^{15} in the

capsule, the rate of depletion of N^{15} with time and also from the penetration profile of N^{15} within the crystal. The ratio of N^{15}/N^{13} is measured by a high resolution mass spectrometer.

One KN_3 specimen in atmospheric pressure of N^{15} was capsuled and was kept at 248°C for about seven days and compared with a control specimen at normal atmosphere. The total decrease in N^{15}/N^{13} in the capsule was measured at the end of the annealing period. The approximate diffusivity of N^{15} is estimated to be about 2×10^{-12} cm^2/sec. This diffusivity is somewhat higher than the corresponding cation diffusivity.

2. Tracer Diffusion of Impurity Anion

To take the advantage of tracer-sectioning technique, the designed experiment will involve diffusion anneal of the KN_3 and RbN_3 specimens in the gaseous atmosphere of radioactive I^{125} (60 days half-life). Diffusion will proceed through all the 6 surfaces of the cubic samples. The specimens will have 4 surfaces parallel to c-axis and 2 surfaces perpendicular to the c-axis. Instead of microtoming, thin sections will be taken by a suitable etchant (a 60-40 ethyl ether and ethyl alcohol mixture etches away .1 m depth in 20 minutes reproducibly). The etched solution will be assayed for radioactivity. Thus two specimens of different dimensions, diffusion annealed at the same temperature, will yield the anion diffusivity in directions along and perpendicular to the c-axis.

Also a number of other important parameters could be obtained from the solution of the diffusion equation under the present boundary conditions:

$$C(x,t) = \frac{C_o}{2}\left[\operatorname{erfc}\left(\frac{x+vt}{2\sqrt{Dt}}\right) + \exp\left(\frac{-vx}{D}\right)\operatorname{erfc}\left(\frac{x-vt}{2\sqrt{Dt}}\right)\right]$$

where $C(x,t)$ = Concentration of the diffusant at a depth x, after a diffusion time t

v = Velocity of the receeding boundary if thermal decomposition at high temperature is not negligible

c_o = Solubility of iodine in KN_3. It will involve the Gibb's free energy g_s for the solid solution of iodine in the azide sample.

Thus this approach is expected to yield valuable information about the decomposition rate at high temperature and the solubility of the anion in addition to the diffusivities of anion along and perpendicular to the c-axis.

III. IONIC THERMO-CURRENT (ITC)

A. Theory

In any ionic crystal, doped with an aliovalent impurity, a certain number of vacancies will be bound to the impurity ions by electrostatic attraction, thus, forming dipoles. By using the technique of ionic thermo-current (ITC), one is able to obtain information about the kinetics of these dipoles. Briefly an ITC experiment involves the following steps:

(1) The sample is first polarized in a static electric field E_p, for a time t_p, at a temperature T_p. E_p, t_p and T_p are so chosen that a significant number of dipoles are aligned with the field.

(2) The sample is then rapidly cooled to a temperature T_o so that the aligned dipoles are frozen. The polarizing field is then removed.

(3) The sample is subsequently warmed up at a constant rate b and the depolarizing current is monitored as a function of temperature.

The depolarizing current density j(T) is given by[7]

$$j(T) = \frac{N_o P e^2 E_p}{kT_p \tau_o} \exp\left(-\frac{E}{kT}\right) \exp\left[-\frac{1}{b\tau_o}\int_{T_o}^{T} \exp\left(-\frac{E}{kT}\right) dT\right] \qquad (6)$$

where N_o = Total number of dipoles per unit volume

P = Dipole moment of the impurity dipole

K = Boltzman Constant

E = Activation enthalpy for the relaxation of the dipoles.

Relaxation time $\tau(T) = \tau_o e^{E/kT}$; a first order process for the depolarization is assumed, i.e., $\frac{dP}{dt} \propto \frac{1}{\tau}$.

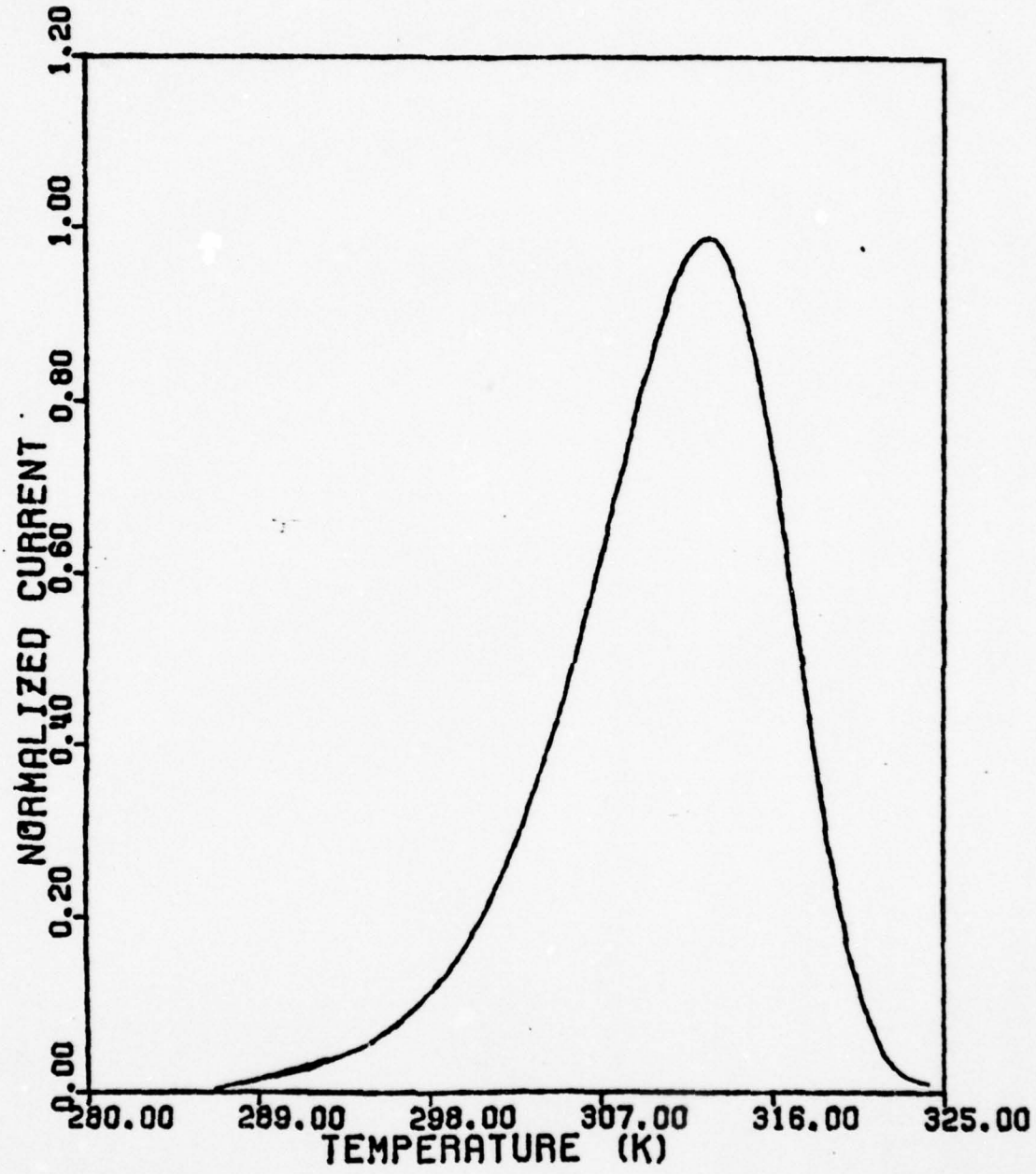

Figure 13. Sketch of a Normalized Theoretical ITC current versus Temperature Plot.

Fig. 13 shows the predicted ITC current as a function of temperature in accordance with eq. (6). The relaxation parameters (E and τ_o) were obtained by several different methods in our study from such ITC profiles:

(1) Since there is "current peak" at a temperature T_m, the partial derivative of j(T) will be zero. This leads to a relation

$$\frac{E}{kT_m^2} = \frac{1}{b\tau_o} e^{-E/kT_m} \tag{7}$$

Thus a plot of ln (T_m^2/b) vs. $1/T_m$ yields E and τ_o.

(2) For $T << T_m$, the factor in the square bracket of eq. (6) approximate to zero and consequently

$$j(t) = \frac{c}{\tau_o} e^{-E/kT} \tag{8}$$

A plot of ln [j(T)] versus $\frac{1}{T}$ yields a straight line of slope -E/k, but τ_o can not be directly determined.

(3) The third method uses the fact that at the time of heating the total polarization, P, left in the sample is the area under the i vs. T curve up to temperature T, i.e. $P(T) \propto \int_T^\infty j(T')dT'$. One then obtains

$$\ln \tau_o + \frac{E}{kT} = \ln \left[\int_T^\infty j(T')dT' \right] - \ln [j(T)] \tag{9}$$

The right-hand side of the equation is obtained graphically and plotted against inverse temperature. τ_o and E are obtained from the intercept and the slope respectively.

(4) An additional method, which is more satisfactory and widely used by us, is to fit the experimental data to the theoretical equation

directly using a computer program and thus obtain the best values of E and τ_o.

B. Experimental

1. Apparatus

Figure 14 shows the schematic of the cryostat, built for ITC, measurements. It consists of two chambers which can be separately evacuated or filled with an inert gas. Inside the inner chamber is a heater can which is noninductively wound.

A platform inside the heater can contains the bottom copper electrode, a diode sensor for heater control and a thermocouple which is attached with insulating varrish to the bottom electrode. All the leads inside the heater, except the top electrode, are routed through copper tubing and out through a vacuum feed-thru.

The top electrode is a small diameter copper wire which is fed through .05 inch diameter stainless steel tubing for support. The stainless steel tubing is held in place by a sapphire disk supplied by Keithly. The sapphire disk also keeps the top electrode electrically separated from the walls of the cryostat. At the top of the stainless steel tubing, the copper wire is connected to a sapphire vacuum feed-thru. The heater connections are routed through vacuum port so that the sample would be shielded from its electrical fluctuation.

The temperature was measured by connecting a digital potentiometer to the thermocouple. The reference junction of the thermocouple was placed in a liquid nitrogen bath. The current was measured by a Keithley 640 Vibrating

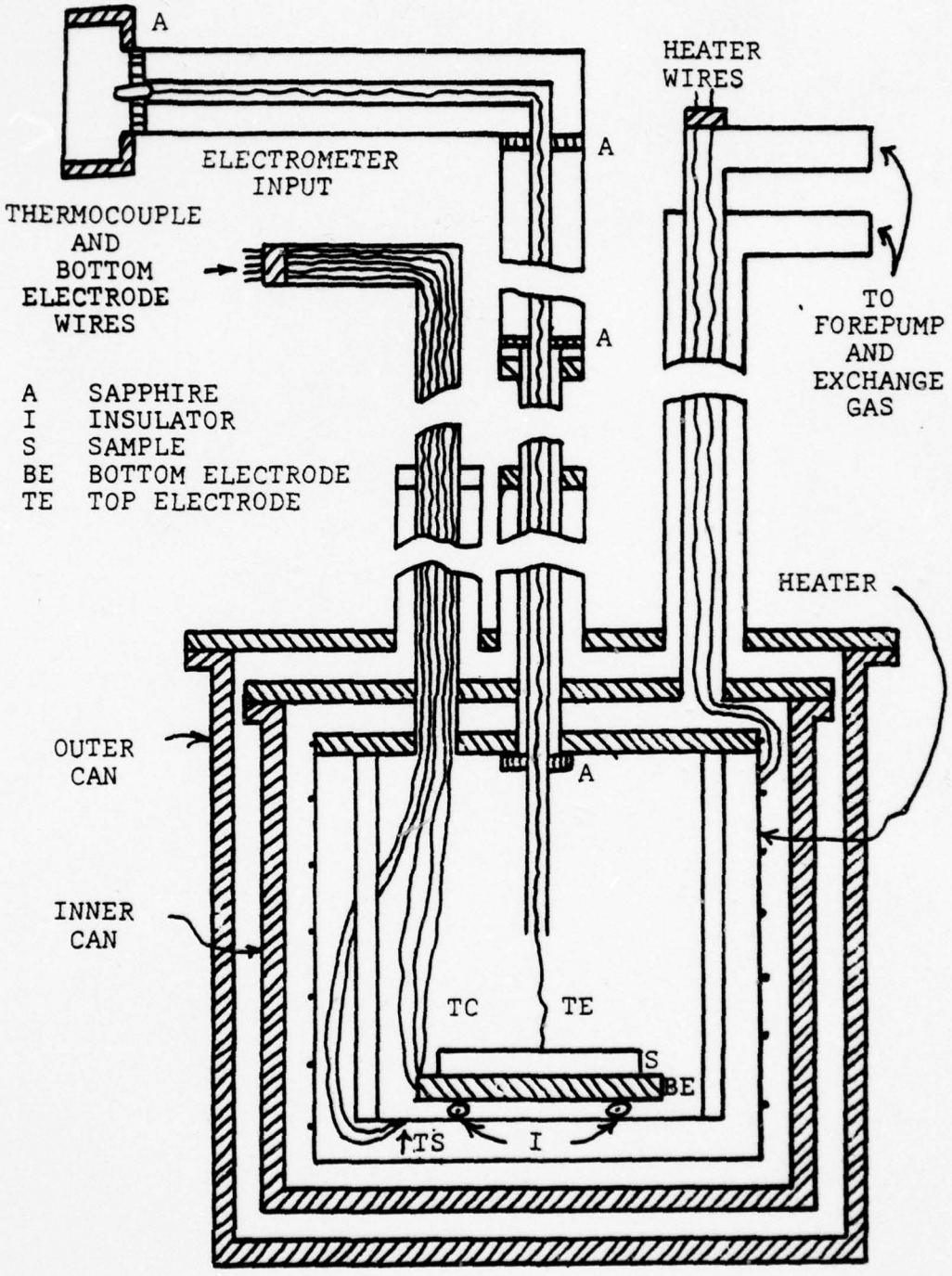

Figure 14. Schematic of the ITC Cryostat.

Reed Electrometer which has the capability of measuring currents of 10^{-16} amps. The electrometer is connected to the top electrode through its separate head. The linear output of the electrometer was used to drive one pen of a dual pen strip chart recorder. The other pen was used to record the temperature.

The heater is controlled by a solid state controller built after the design of Manning[8], with some modifications to allow for the different resistance of this heater. The controller, besides holding the temperature, is capable of increasing the temperature at a linear rate.

2. Sample Preparation

One RbN_3 and five KN_3 samples doped with various impurities were used for ITC measurements. All the samples were grown from solution by adding chloride salts of the desired dopants to the saturated solutions of RbN_3 or KN_3. A spectrochemical analysis, performed by Jarrell-Ash Company, showed that the concentration of the respective dopants in RbN_3:Ba, KN_3:Cu, KN_3:Ca, and KN_3:Ni was 0.01% → 0.1%. The concentration of Co in KN_3:Co was higher, 0.1-1%. The KN_3:Pb sample is also believed to have impurity content of the order of 0.01% → 0.1% since it was grown in the same way. This sample was not sent for analysis to Jarrell-Ash Company and an attempt to determine the impurity content by polarographic method in our lab failed.

For electrical contacts two sides with larger surface areas of the polished samples were coated with high purity silver paint. A piece of mylar was then attached to each side, and then its surface was also coated with silver paint. After cutting the mylar to a rough shape of the sample, the sample was mounted to the bottom electrode using silver paint for a good electrical connection and mechanical stability. The top electrode was then

silver painted to the top of the sample and all the cans were sealed and both chambers evacuated.

3. Measurements

The top and bottom electrodes were electrically connected together and the cryostat was placed in a dewar of liquid nitrogen. To remove any water which could be present in or on the sample, the temperature of the inner chamber was raised to 120°C while the chamber was still evacuated. After about one hour the outer chamber was filled with helium gas, the heater was turned off, and the sample was allowed to cool. Once the temperature dropped below 0°C, a dc field was applied across the sample. To remove the possibility of polarizing the sapphire disks, the top electrode and the outside of the cryostat were connected together.

The inner chamber was now filled with helium and the sample was allowed to cool rapidly until the temperature was about 100 K. The field was removed and the outer chamber evacuated. The bottom electrode was grounded to the cryostat and the electrometer was connected to the top electrode. The strip chart recorder was tested and zeroed and the analogue output of the electrometer was connected so as to drive one of the pens. The heater was set for a fast rate, 0.3 K/sec, so that the temperature could be swept quickly in order to find any peaks that were present. If no peak was found then the temperature at which the field was applied (polarizing temperature, T_p) was raised until one was found.

After a peak was located, several passes were run without changing any variable to check on its reproducibility. Once its reproducibility was established, the polarizing temperature was changed to temperatures above and

below the temperature where the maximum current occurred (T_m) to see if the curve shifted with the polarizing temperature.

Once it was justified that T_m was independent of the polarizing temperature, then different fields were applied. This resulted in larger peaks occurring for the higher fields. The rate of heating was also varied to find out if a faster rate resulted in the peak shifting to a higher temperature. All these checks were run so as to ascertain reproducibility and to establish that the peak observed was actually a true ITC peak and not a space charge or a surface response causing the peak.

4. Data Analysis

τ_o and E, relaxation parameters for the relaxation process of the dipole orientations were obtained in accordance with equations (7), (8), (9). As mentioned earlier more satisfactory results were obtained by a computer fit of the experimental points to the equation (6). The program employed uses the least squares fitting technique of minimizing the squares of the deviations:

$$d^2 = \sum_{j=1}^{n} [i_j(exp)-i_j(cal)]^2$$

where

n = the number of data points

$i_j(cal)$ = the current calculated from the ITC equation for the temperature of the j^{th} point

$i_j(exp)$ = the measured current

d = the deviation

There are three parameters to be fit, τ_o, P_o and E. This is reduced to two parameters P_o and E by using the equation (7). The value of T_m is varied

over its small temperature range until the best fit is obtained.

C. Results

ITC runs of all the differently doped samples showed the same general behavior: a single peak which was independent of the polarizing temperature, and another one at a higher temperature which would shift with the polarizing temperature. Upon applying different fields to all of the samples, the peak which was independent of T_p, exhibited a direct dependence on the magnitude of the polarizing field. When a second check was applied, that is, changing the rate of heating b, it was found that the peak would shift to a higher temperature for a faster rate. Since the maximum temperature of the peak was independent of the polarizing temperature T_p, the peak is not due to space charge effects, but due to a thermally stimulated depolarization process. The peaks were analyzed assuming first order kinetics and good fits were obtained.

The data and the calculated fits are shown in Figures 15 through 20. The boxes are the experimentally determined points and the line is the calculated fit. The vertical scale is found by taking the logarithm of the ratio of the current for each point to the maximum current. It should be noted that the current for all the samples ranged from 2×10^{-13} to 7×10^{-12} amps. The results of the least squares analysis are shown in Table 7.

Excellent fits were obtained for Cu^{+2} in KN_3 and Ba^{+2} in RbN_3. It was possible in these cases to separate the upper T_p dependent peak from the ITC peak especially in the RbN_3 samples. The values of τ_o and E seem very reasonable for both samples.

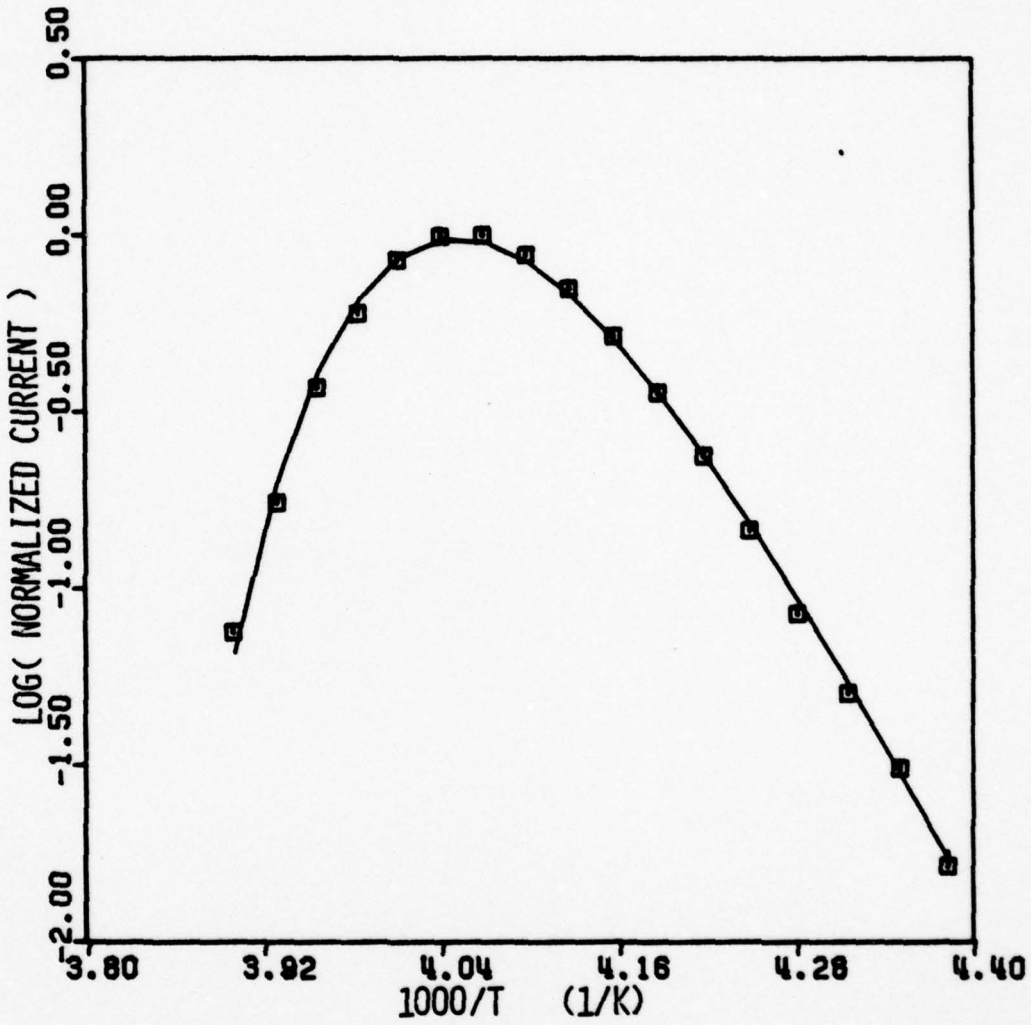

Figure 15. ITC Peak for RbN_3 Doped with Barium.

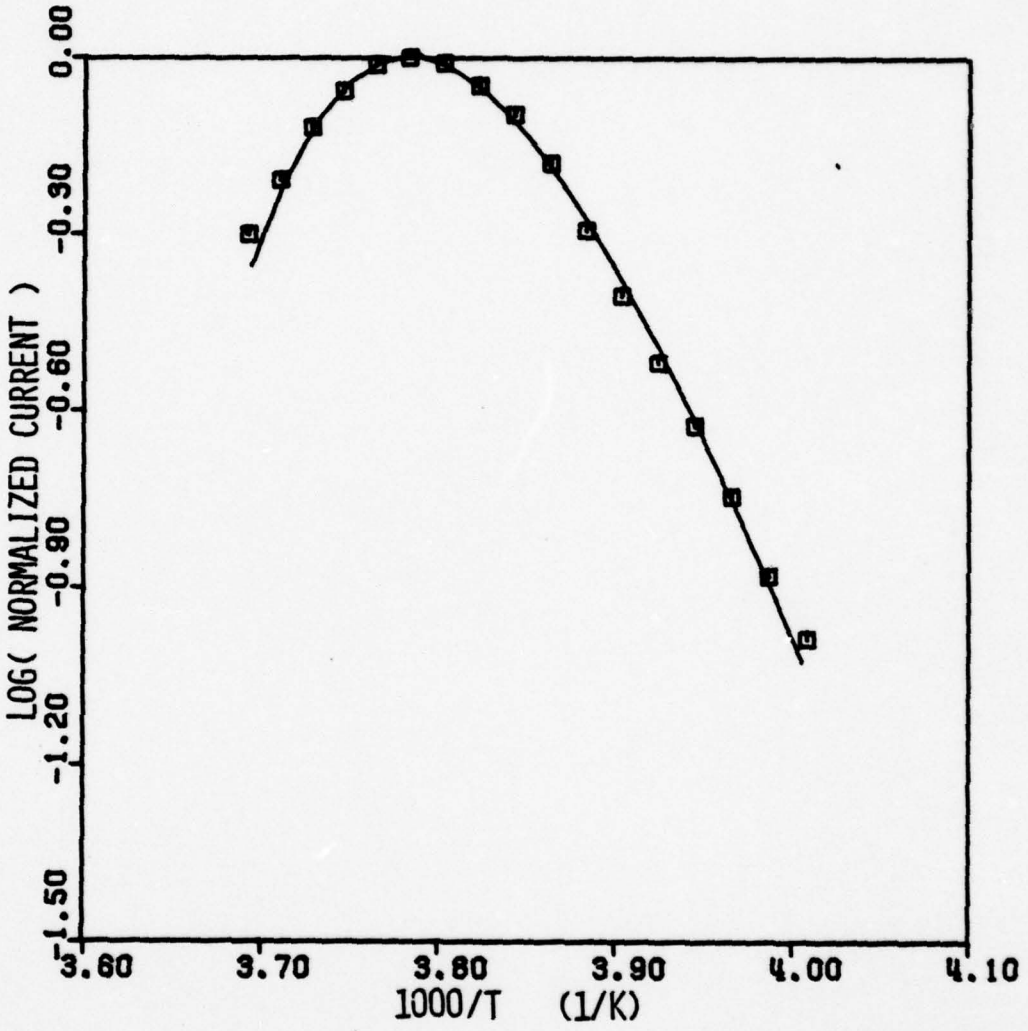

Figure 16. ITC Peak for KN_3 Doped with Copper.

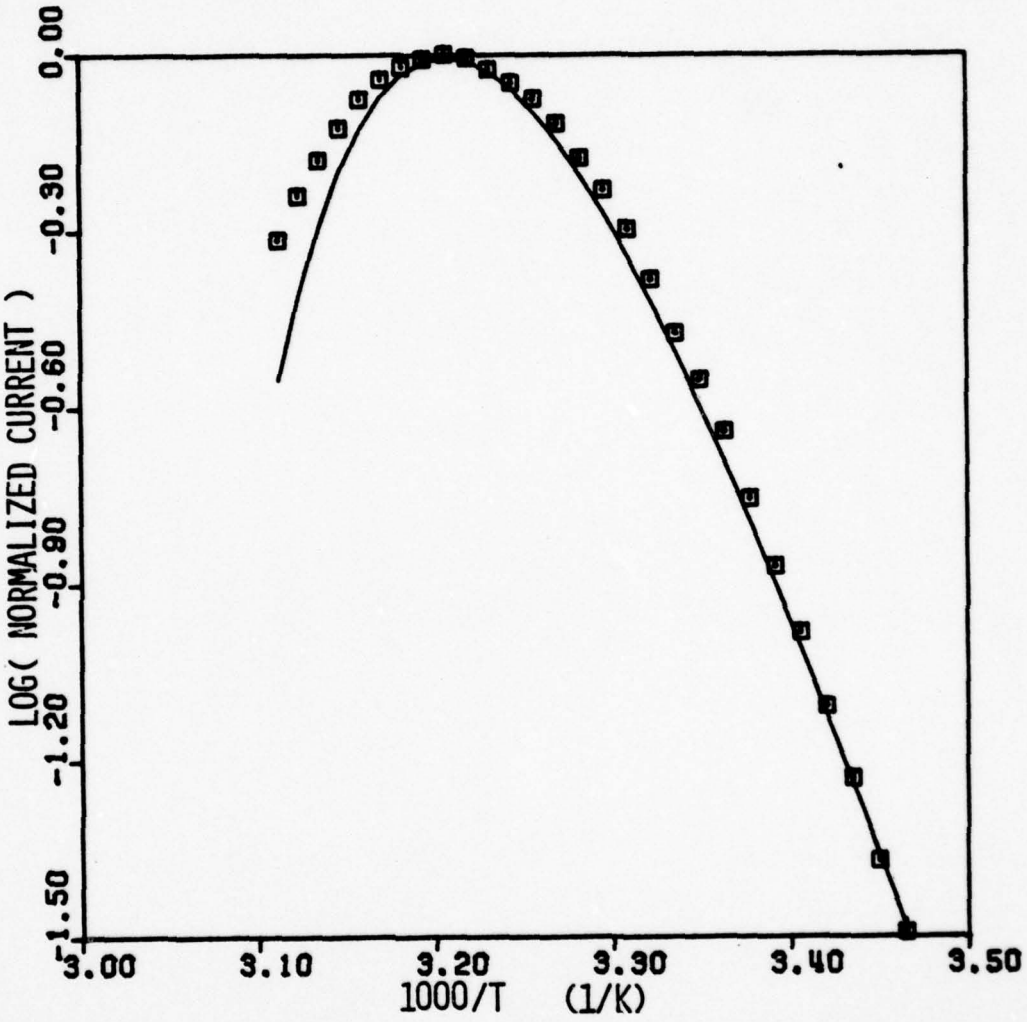

Figure 17. ITC Peak for KN_3 Doped with Calcium.

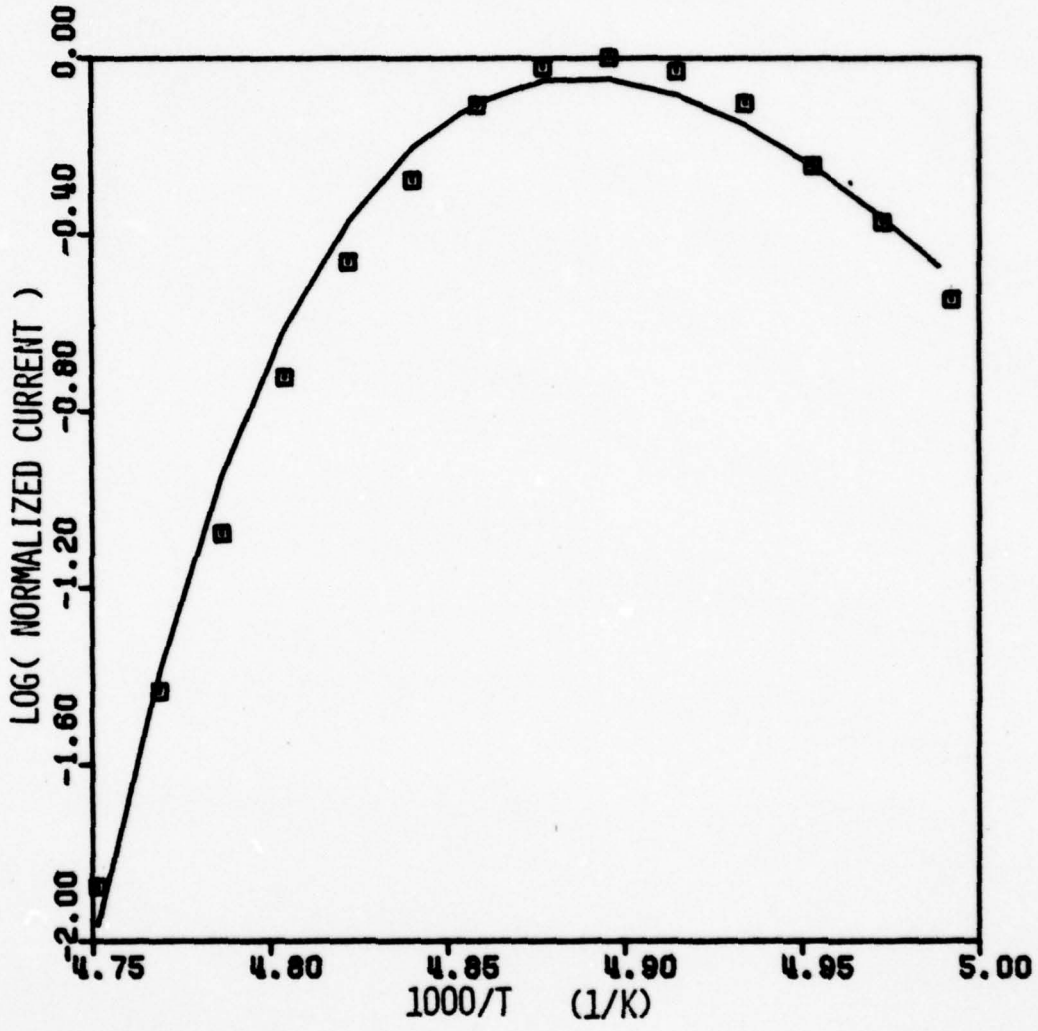

Figure 18. ITC Peak for KN_3 Doped with Lead.

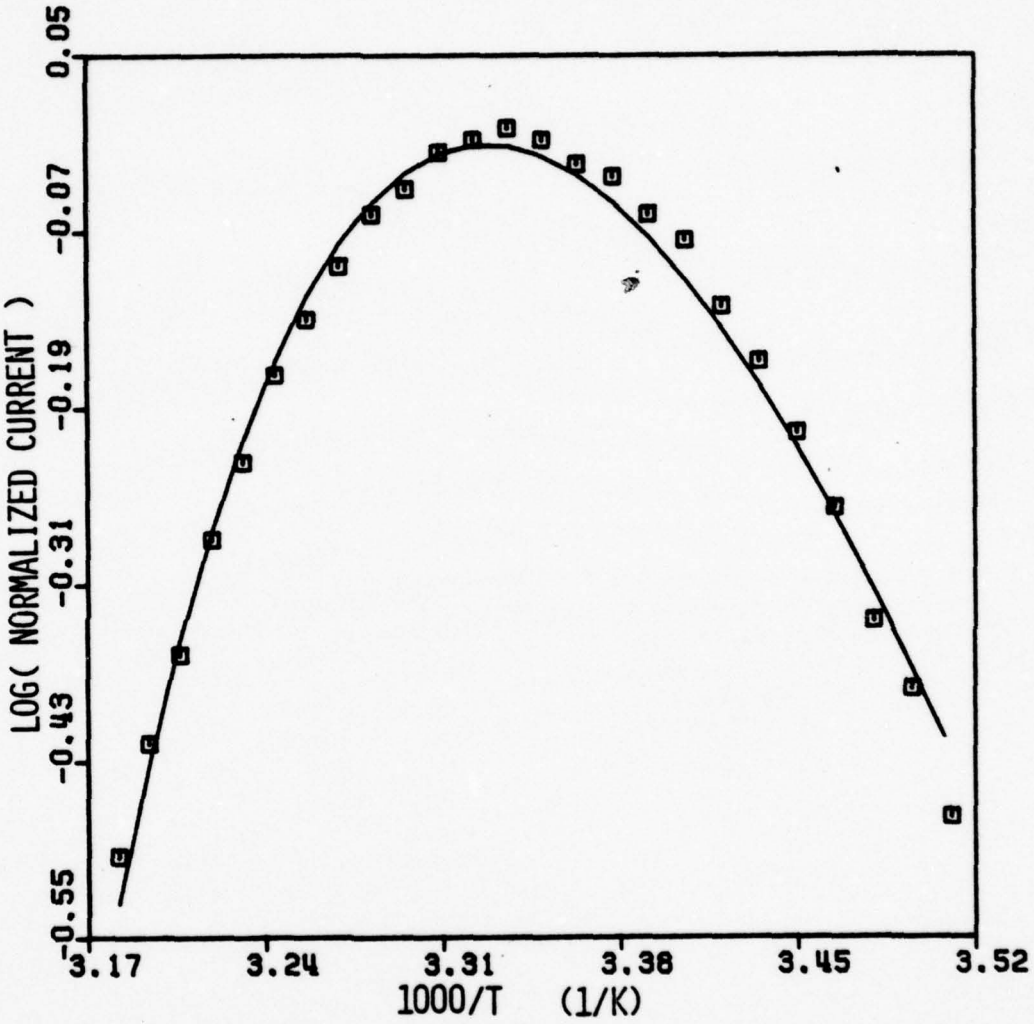

Figure 19. ITC Peak for KN_3 Doped with Nickel.

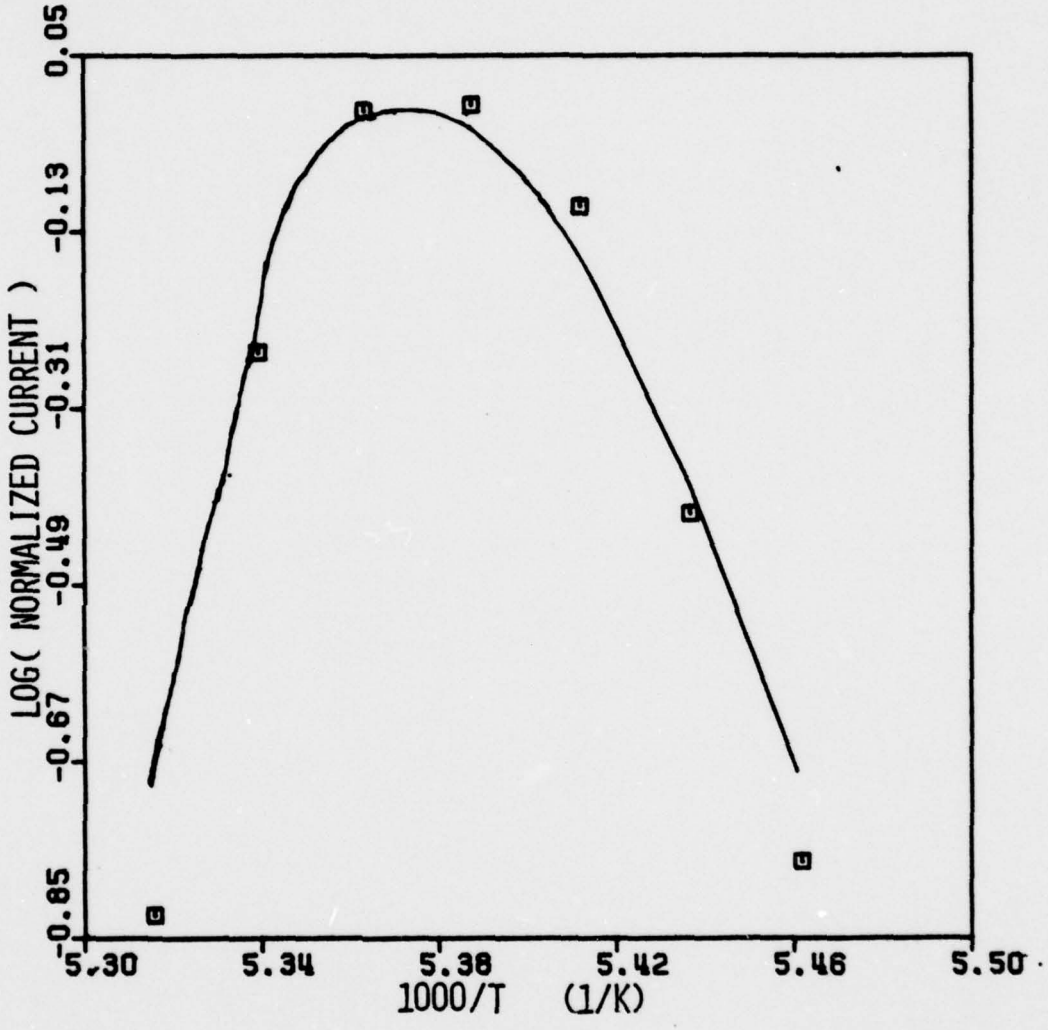

Figure 20. ITC Peak for KN_3 Doped with Cobalt.

A good fit was obtained for calcium, lead, and nickel doped KN_3. The calcium doped KN_3 curve does have a rather large deviation from the calculated line at high temperatures. This is due to a large T_p dependent peak which could not be totally removed from the region where the ITC peak occurs. Therefore, the current did not return to zero at the high temperature edge. For lead doped KN_3 the fit is reasonably good. The curve did return to around zero on the high temperature edge. The fit which was found for nickel doped KN_3 does not seem to be as good a fit when compared to the other results. This peak was very broad for this temperature range. It is possible that the upper T_p dependent peak was interferring, but this upper peak was not visible in this sample. Also, the current did return to zero at the higher temperatures. The values of .49 eV for the depolarization energy and 1.07×10^{-6} sec for the relaxation time do not seem as reasonable, when compared to the values obtained for the previous dopants.

Even though the fit for cobalt doped KN_3 is not bad, the values of 1.45 eV and 3×10^{-38} sec for E and τ_o seem unreasonable. This curve is extremely sharp and was not found until the field was applied within $\pm$ 2°K of its T_m. The peak was also found when the field was applied at a higher temperature and the temperature lowered to below T_m, but it was much smaller in amplitude. Several runs were made to try and broaden the peak by using different rates but the number of points derivable from the data is still small for the 5°C temperature range. Therefore these values could be uncertain due to statistical errors using the least squares fit. Also, it was found that the concentration of Co-doped crystals was at least 10 times higher than those of other doped crystals, a factor that may contribute to complex kinetics giving rise to uncertainties.

It will be worthwhile to record an observation the origin of which is uncertain. Even without application of the field a dual peak occurred around 226 K in pure and doped KN_3. The positive peak begins first and is small (10^{-14} amps) and the negative peak is larger (3×10^{-4}) for one sample. This almost looks like the self polarization peak seen by Taylor[9] in Ammonium halides at the low temperature phase transition. But no phase transition for KN_3 at low temperature is reported. Regular ITC of all these samples were studied by application of an electric field.

D. Discussion

The relaxation parameters (Table 7) are quite reasonable and are of the same order as one gets for impurity-vacancy relaxation in other ionic systems. For example, in case of CaF_2 system relaxation times of the order of 10^{-8} to 10^{-19} have been reported by Kitts.[10] The relaxation parameters for Co-doped samples are unusual, but as noted before they are also suspects of uncertainty. Disregarding this case, an interesting size effect can be seen for the dopants by comparing their ionic radii with the best fit obtained for the relaxation times and energies (Table 8). As ionic radius of the impurity increases the activation enthalpy for the relaxation modes of the impurity dipoles monotonically increases, but τ_o decreases correspondingly. Thus the dipolar relaxation rate increases with the decreasing size of impurity ions. As noted before, the other significant observation of single ITC peaks in samples doped with these impurities not only implies that only nearest-neighbor vacancy-impurity complexes are formed but each of them has a single relaxation mode. The extensive studies of the dielectric relaxation in NaCl by Dreyfus[11] have

TABLE 7. ITC Results for KN_3 and RbN_3.

Host	Dopant	Heating Rate (K/sec)	E (V/cm)	T_p (K)	T_m (K)	τ_o (sec)	ξ (eV)
KN_3	Cu^{+2}	0.10	804	247	264	3.79×10^{-12}	0.70
	Co^{+2}	0.04	495	187	186	3.01×10^{-38}	1.45
	Ca^{+2}	0.1	870	316	312	4.86×10^{-12}	0.77
	Ni^{+2}	0.11	385	305	300	1.07×10^{-6}	0.49
	Pb^{+2}	0.05	1100	204	204	2.18×10^{-20}	0.88
RbN_3	Ba^{+2}	0.08	1000	250	247	1.32×10^{-12}	0.68

TABLE 8. Relaxation Modes of Impurity Dipoles in KN_3.

Dopant	Ionic Radii (Å)	τ_o (sec)	E_a (eV)
Pb^{+2}	1.21	2.18×10^{-20}	.0.88
Ca^{+2}	0.99	4.86×10^{-12}	0.77
Cu^{+2}	0.92	2.54×10^{-12}	0.70
Co^{+2}	0.72	3.01×10^{-38}	1.45
Ni^{+2}	0.49	1.07×10^{-6}	0.49

led to similar conclusions.

The reorientation of the impurity-vacancy dipoles can be understood in terms of the various jump frequencies of the impurity ions and host ions with the vacancies. If we neglect the anistropy of KN_3 structure which is nearly cubic the following jump frequencies are involved in the orientational changes in the nearest neighbor impurity-vacancy dipoles:

ω_1 = n.n → n.n; jump frequency of the nearest neighbor (n.n) host ion to the n.n vacancy

ω_2 = Direct interchange jump between the impurity ion and n.n vacancy

ω_3 = n.n.n → n.n; jump frequency of the next nearest neighbor (n.n.n) vacancy with n.n host ion

ω_4 = n.n → n.n.n; jump frequency of the n.n vacancy with n.n.n host ion

In KN_3 and RbN_3, as in almost all ionic systems, ω_2 is the slowest and is the rate limiting frequency for impurity diffusion. The reorientation of the impurity-vacancy associated pair, then, can be achieved in two ways:

(1) A single ω_1 jump

or (2) A ω_4 jump followed by a ω_3 jump

For both these possibilities, a simple argument will indicate that host ions in general will need more energy to make reorientation jumps in the neighborhood of an impurity with larger ionic radius due to the polarizability and coulomb fields. In case of NaCl Dreyfus[11] concluded that $\omega_3 > \omega_4 >> \omega_1$ to explain the single mode of dipolar relaxation and the size effect of the impurity ions. It appears that similar mechanism is involved for the dipolar relaxation in KN_3 and RbN_3.

However, for the anistropic structure of our system a large number of jump frequencies are involved due to the possibility of non-equivalent jumps along and perpendicular to the c-axis. A model calculation is being developed to understand the role of anisotropy on the relaxation processes. It will be interesting to see whether the fact that motion enthalpies (for ω_2) are almost same in direction parallel and perpendicular to the c-axis (Appendix-1) is an indication that the anisotropy in other jump frequencies is also small enough to predict single mode of relaxation.

IV. CONDUCTIVITY IN RbN_3

The investigation of the conductivity of RbN_3 was undertaken to extend the temperature range of our earlier study[3] and to determine the conductivity profile of the crystals from the same batch used for diffusion studies. These measurements were performed as before with an ac field of 1 kHz to prevent any modulation effects which space charge in dc measurements can produce. This led to some unexpected and interesting observations. These were pursued in detail by studying the dc conductivity and the frequency effect on the ac conductivity.

A. AC Conductivity (1 kHz)

The apparatus and the general procedure for conductivity measurements are described in the earlier report[3] and Wagner's thesis. Several measurements at 1 kHz were made by measuring the conductivity of the specimens while warming up from room temperature to about 255°C and then during cooling cycle. The specimen temperature was raised by 5 to 10°C at a step and about half hour to one hour waiting period to reach thermal equilibrium was allowed before making a measurement. Fig. 21 is the conductivity profile of such a typical static run. These results are essentially similar to Wagner's. The noteworthy features of these runs are:

(1) the first heating run on each sample showed lots of structure, but the bumps seen by Denemar[12] in most of his runs for KN_3 are absent.

(2) the cooling run shows very little structure and two regions are observed which are believed to be the extrinsic and intrinsic regions.

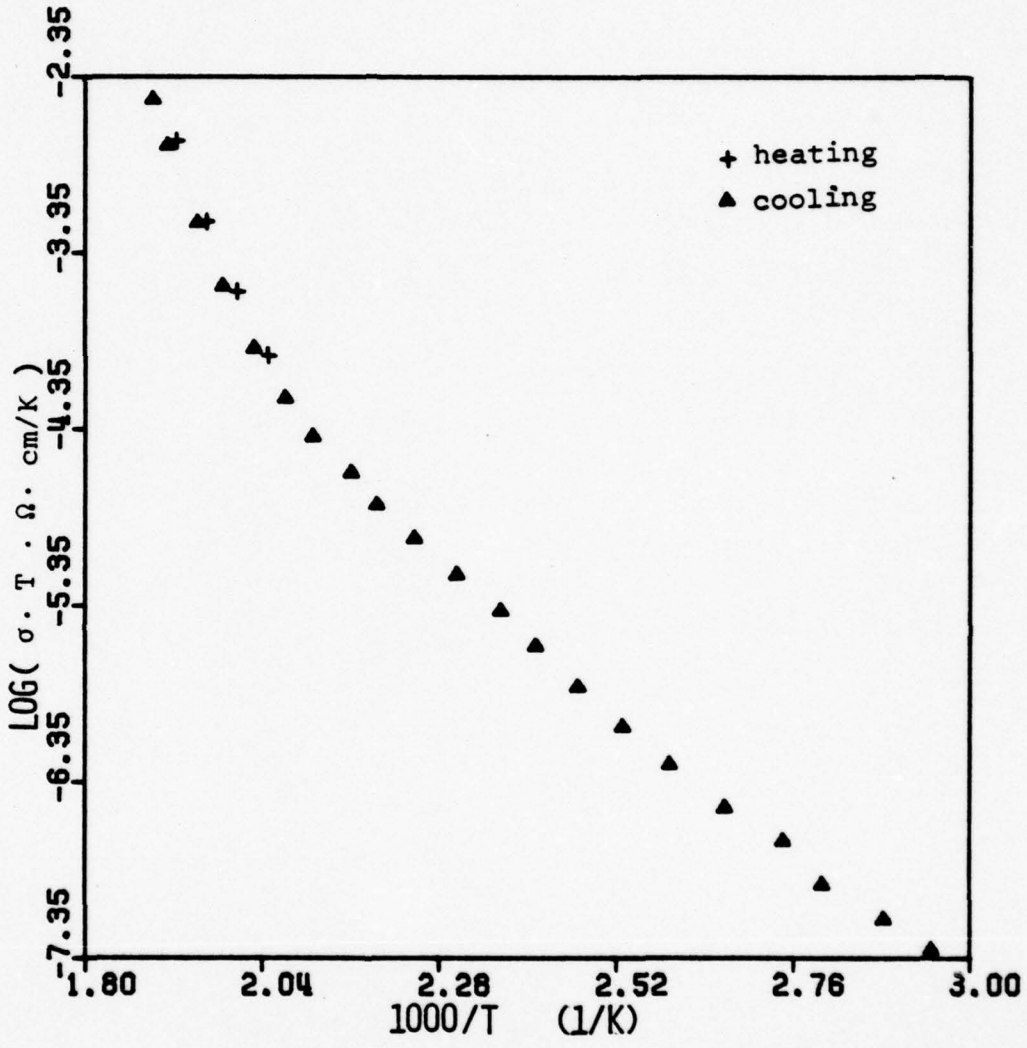

Figure 21. Arrhenius Plot of RbN_3 Conductivity, Static Heating and Cooling Run at 1 kHz.

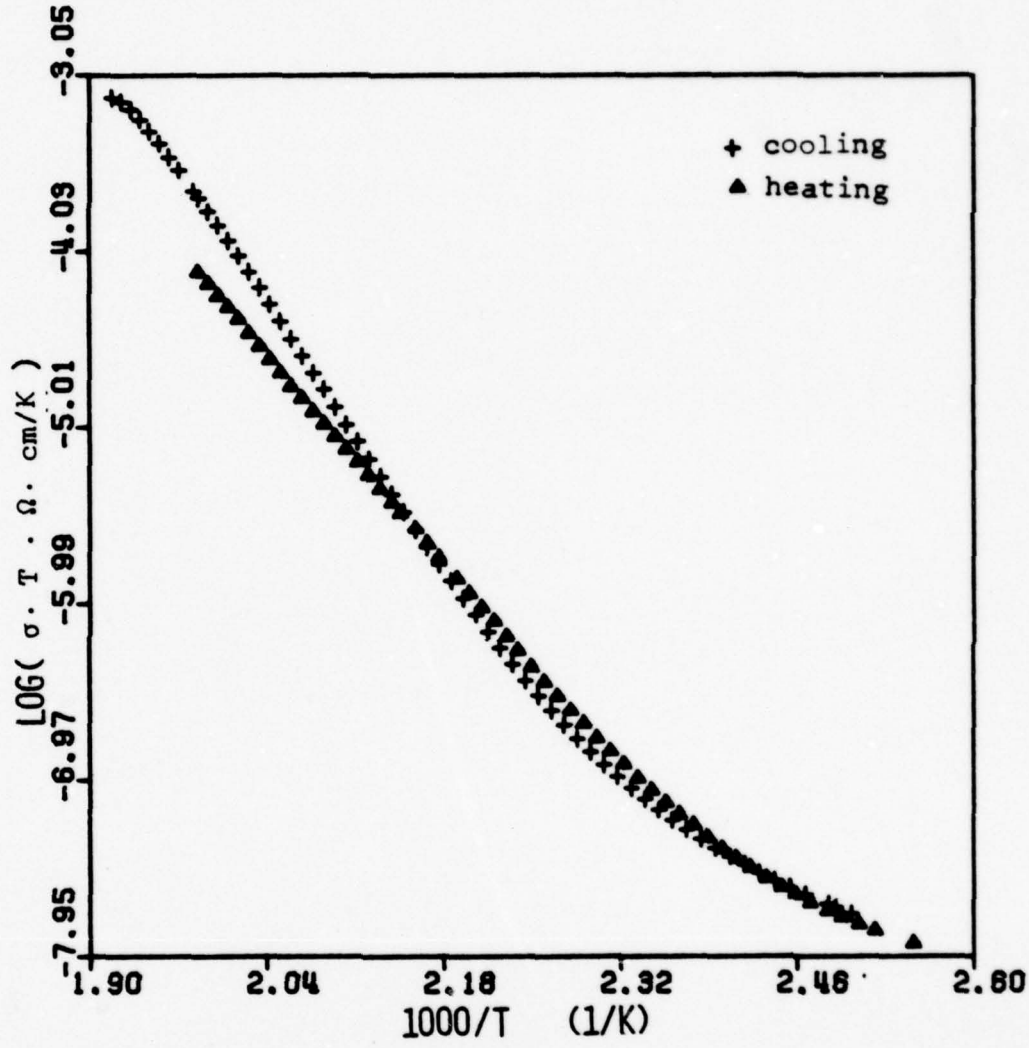

Figure 22. Arrhenius Plot of AC Conductivity in RbN_3 Dynamic Heating and Cooling Run.

(3) subsequent heating runs on the same sample result in the same type curve as in the cooling run. Since RbN_3 is hygroscopic and the samples are cut from bulk crystals using a water solvent string saw, it is possible that during the first heating run the samples experienced a drying out effect. A thermal annealing process may also take place, resulting in this improved performance.

(4) there is still some hysteresis present between heating and cooling runs, expecially for samples which are taken to temperatures above 255°C.

Besides the static runs, several "dynamic" runs were performed where the temperature was increased or decreased continuously be using a programmable temperature controller. The average rate of temperature change was about 15°C per hour. Measurements were taken and recorded approximately every degree. The results of a dynamic a.c. conductivity run are shown in Fig. 22. It is observed that the profile is better defined due to the large amount of data. Hysteresis effect is also much smaller. The possible reason for the improved results could be that the total time the sample is held at temperatures above 210°C is shorter. During static runs the sample temperature is raised by five degrees and held for about one hour. Whereas for the dynamic run the rate of heating is 15°C per hour. The increased time at higher temperature could result in some decomposition at very high temperatures and the possibility of electrolytic action from Ag diffusing from the Ag electrodes, may cause some uncertainty as observed by Abbink[13] in his study of σ in AgCl.

The high temperature region for the plot of log σT versus $1/T$ is believed to be exhibiting intrinsic behavior, and yields an activation energy 1.65 eV for a total of eight runs.

Almost all the static runs showed a two segmented Arrhenius plot, whereas under dynamic conditions the plots are smoother. The activation enthalpy for this lower segment yields a value between . 5 and .7 eV. If one identifies the lower segment as the extrinsic region due to the background impurities, then the average activation enthalpy (.6 eV) should correspond to the activation enthalpy of motion H_m. This value is in the range of what Wagner found earlier, but must be taken with caution due to the observations in the following section.

B. Frequency Dependence of Conductivity

Since the temperature range of the present investigations was extended to much lower temperature, it was decided to check the frequency dependence of the conductivity, though earlier work did not show any appreciable effect. The results for one sample are seen in Fig. 23. The "plateau" seen for 1 kHz is significantly raised for 10 kHz at low temperature.

Such frequency effect arises from the response of impurity vacancy dipoles to the ac field. If one considers the effect of the alternating field on the reorientation of the dipoles, one is led to a "Debye type loss peak" which has been explicitly worked out be Lidiard[14]. He finds that, for a NaCl structure with a single species of nn dipoles

$$\tan \delta = \frac{8\pi a^2 e^2 N_i}{3\epsilon k} \frac{P}{T} \left[\frac{\omega\tau}{1 + \omega^2\tau^2} \right]$$

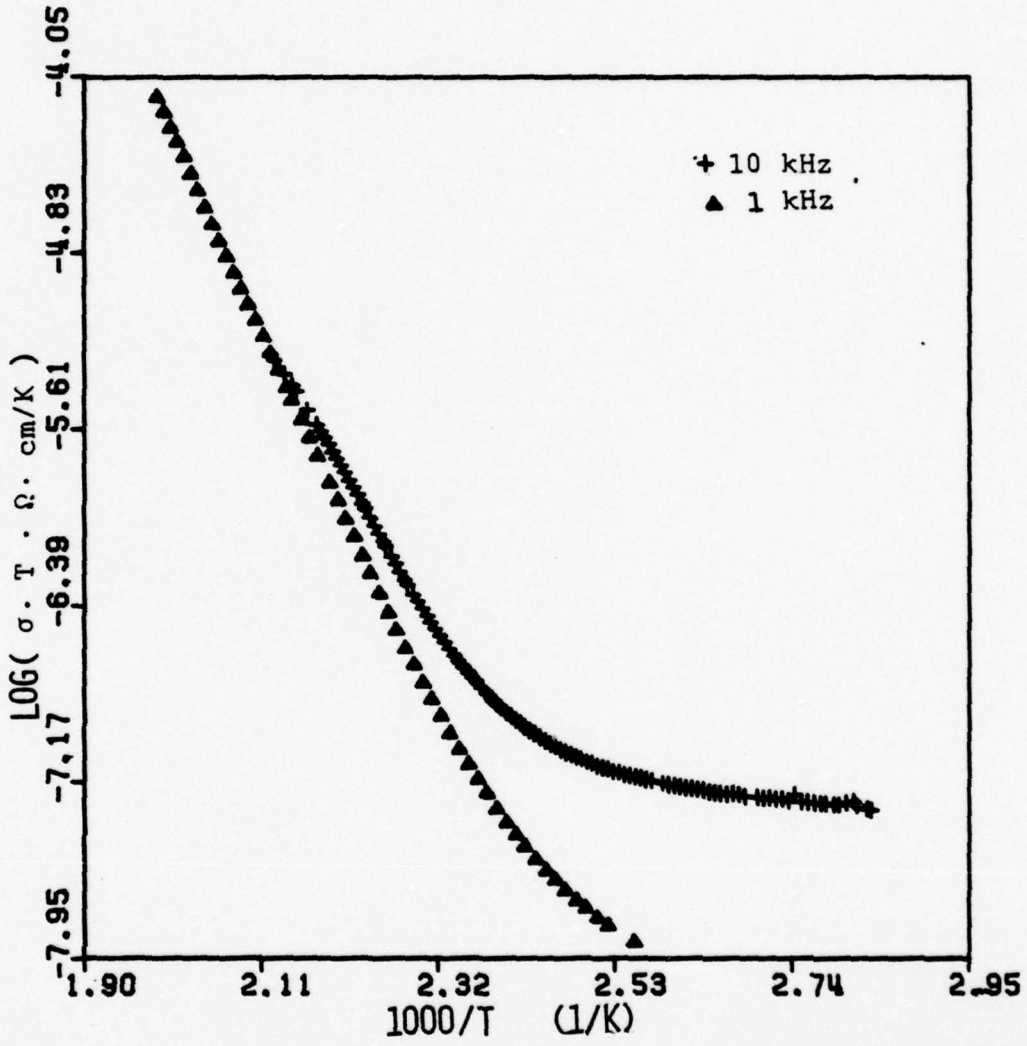

Figure 23. Arrhenius Plot of AC Conductivity in RbN_3 at 1 and 10 kHz.

$$\sigma T = \frac{2a^2e^2N_iP}{3k} \cdot \frac{\omega^2\tau^2}{1 + \omega^2\tau^2}$$

$$\tau = \frac{1}{2\omega_1 + \omega_2}$$

where

a = the lattice spacing,

N_i = the number of impurity ions per unit volume,

P = the degree of association which is temperature dependent,

ω = the frequency of the applied field,

δ = the phase angle,

ω_1 = the jump frequency for a vacancy from an nn site of an impurity to another nn site

ω_2 = *the jump frequency for the direct interchange of a vacancy and* in impurity.

This leads to:

1. a dielectric loss, tan δ, which is governed by $\frac{\omega\tau}{1 + \omega^2\tau^2}$. Thus a Debye peak occurs when $\omega \approx \tau$ in a plot of log (tan δ) versus log ω;
2. a bump or peak in a graph of the log (tan δ) versus T;
3. a broad bump in a graph of the log σT versus $\frac{1}{T}$.

This could be the reason for the "plateau" which is found in some of these "pure" crystals since they contain various aliovalent impurities of the order of 50 ppm. The combination of these different Debye peaks could result in the "plateau" seen. The "plateau" observed also shows the right trend in

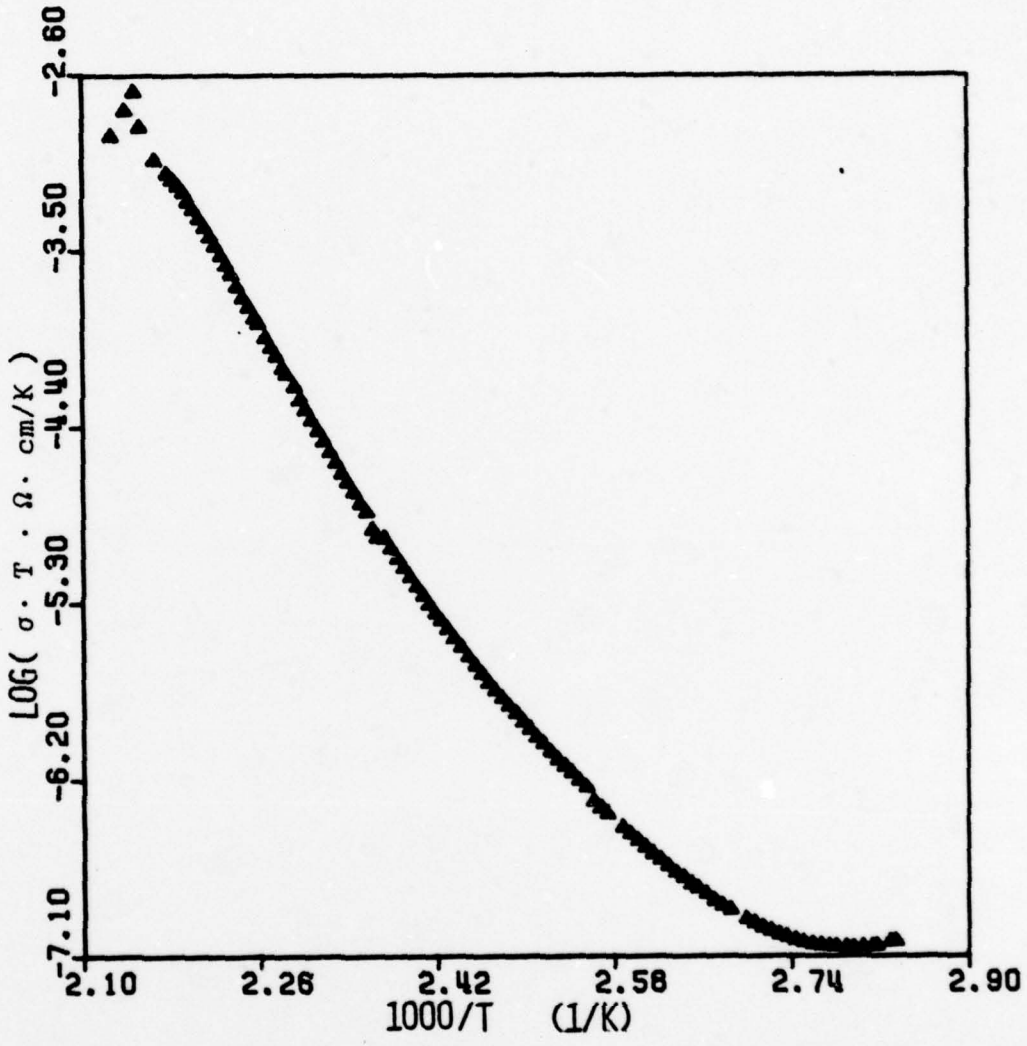

Figure 24. Arrhenius Plot of the DC Conductivity in RbN_3.

in that at higher frequencies the "plateau" moves up to higher temperatures, which follows from the condition that $\omega\tau = 1$.

From ITC measurements, the value of the relaxation parameters of a Ba^{+2} doped RbN_3 sample have been determined, ($\tau_o = 1.3 \times 10^{-12}$ sec and E = .68 eV). Using the above values for a 1 kHz ac field a Debye peak is expected in the region below 100°C. If one assumes that many of the background impurities have relaxation parameters comparable to those obtained for barium, then the combination of all their peaks could result in the observed "plateau."

C. DC Conductivity

To stay away from such effects caused by an ac field, dc conductivity measurements were performed on the same samples. The conductivity rig was modified so that ac and dc conductivity measurements could be carried out simultaneously. After a sample was mounted a 22.5 volt mercury battery and Keithley 610-C electrometer were connected in series using shielded cables. To the output of the electrometer, a digital voltmeter was connected for a quick and accurate reading of the current. Fig. 24 shows such a heating run. The pronounced "plateau" seen in the 10 kHz run is not evident in this case.

D. Discussion

Most conductivity measurements in ionic crystals are performed with 1 kHz ac field[14]. This avoids the space charge effects in a dc measurement, but as the previous discussion show even the presence of "small" amount of aliovalent impurities may give rise to a "plateau" due to the orientation of the impurity-defect dipoles. The low temperature segment of the Arrhenius

plots, thus may contain two contributions: (1) enhanced conductivity due to the mobility of the unassociated vacancies generated by the aliovalent impurities (much greater than the concentration of thermal vacancies) and (2) a "Debye loss peak" due to orientational effects of dipoles. The latter is absent from a dc measurement of conductivity, but one has to be careful about the space charge effects.

This is not much of a problem for some systems like alkali halides and silver halides where the impurity content in pure crystal is less than 1 ppm. The purest crystal of RbN_3 has polyvalent impurity content of about 20 ppm. So as a procedure the dc conductivity and ac conductivity at 1 kHz and 10 kHz were measured simultaneously in several samples. The results of those "pure" samples for which frequency dependence was not significant and dc conductivity showed similar profiles were considered. The average of 4 such determinations yield an activation enthalpy (H) of 1.71 eV in the intrinsic region and 0.68 eV for the extrinsic region. The latter is the motion enthalpy (H_m) for the cation vacancies. In the intrinsic region, $H = H_F/2 + H_m$ where H_F is the formation enthalpy of the Schottky defects. H_F is then estimated to be 2.06 eV. These values are believed to be more well defined than these reported earlier.

A systematic investigation of the effect of intential doping of divalent impurities (of varying concentration) on the conductivity was not possible due to the extreme difficulty in growing large enough doped crystals. Only a few doped crystals were grown which were suitable for ITC measurements but not for conductivity experiments.

V. SUMMARY

The aim of this project has been to investigate the crystalline defect structure, their transport and the interactions between the defects and chemical impurities in alkali azides. The results demonstrate that by applying a closely coordinated effort in which solid state techniques, such as the measurement of electrical conductivity, tracer diffusion, and ionic thermocurrent (ITC) were employed, the basic knowledge of the solid state of the materials as complex as alkali azides can be obtained. Also, the details of the physical nature of these solids can be understood in the general framework of Lidiard's Theory[14] of ionic solids.

A major effort in this project was to grow large and good quality single crystals of a variety of alkali azides by a number of different techniques. Excellent quality single crystals of KN_3 (5 cm long, about 2 cm dia) were grown by Kyropolous technique and RbN_3 crystals ($2cm^3$ dimension) by a special evaporation technique. The crystals were characterized by x-ray studies. A special etching solution was developed to reveal the dislocation content of the as-grown crystals to be about $10^6/cm^2$.

Earlier study of the electrical conductivity has been supplemented by measuring the conductivity in RbN_3 over a wider temperature range both by ac and dc methods. This has established that dc conductivity reflects the proper charge transport mechanism as in ac methods a frequency effect is superposed due to the reorientation of the impurity-vacancy associated pairs.

The tracer diffusion of Rb^+ and Ag^+ in RbN_3 and Ag^+ in KN_3 (along with earlier studies of K^+ and Na^+ in KN_3) yielded cooperative data to understand

the details of ionic defects and their transport. The results of these investigations have established that the defect structure in these systems is Schottky type and the cations migrate by a vacancy mechanism. The thermodynamic parameters for the formation and migration of defects are now well established. Of considerable interest is the anisotropy in charge and mass transport along and perpendicular to the c-axis in the body-centered tetragonal structure of this system.

Impurity-defect interactions have been studied in both KN_3 and RbN_3 doped with a number of divalent ions by using the ITC technique. The analysis of the relaxation time and the activation enthalpy indicate that impurity-vacancy associated pairs reorient by a single relaxation mode. One of the most significant findings of the ITC studies is that the relaxation rates decrease as the ionic radius of the dopant increases. It is concluded that the aliovalent impurities form dipolar complexes with the nearest neighbor vacancies, they reorient by the interchange jumps of the vacancies with the neighboring host ions. The decrease of relaxation rates with increasing ionic sizes of the impurity is due to the polarizability and coulomb fields.

Thus, it is seen that solid state properties of the alkali azides are very similar to those of a much simpler ionic system like NaCℓ which has been extensively studied over many years.

Further work in several directions is warranted to complete our understanding of the defect properties in this system and then to strive for a correlation between these basic properties and the phenomena like fast solid reactions which are characteristic to azides. In addition to the efforts planned and continued in our laboratory, it has been possible to

develop collaborative work with the scientists of some other institutions. These are indicated below:

1. The ITC measurements will be used extensively to study the impurity-defect interactions in greater detail. The solubility and the precipitation kinetics of the dopants will be monitored by the ITC measurements of the highly doped and quenched specimens.
2. The planned anion diffusion in this system will complete the description of ionic transport. It would be interesting to see whether the rapid evolution of nitrogen during thermal decomposition at high temperature is in anyway diffusion limited.
3. On going experiments on the study of anisotropic diffusion of Ag^+ in KN_3 will be an important supplement to our observations on the role of anistropy on the ionic transport in RbN_3.
4. The work of Dr. Sam Trevino, N.B.S. on the lattice vibrational modes of KN_3 and RbN_3 by neutron scattering technique will help us to understand the anisotropic properties in detail.
5. Dr. Larry Cain, now at Davidson College, N. C. has agreed to determine the elastic constants of both KN_3 and RbN_3 by ultrasonic technique. It will be interesting to see whether the anistropy observed in the attempt frequencies (generally taken to be the Debye frequency) for the diffusion along and perpendicular to the c-axis (Appendix-1) is supported by a similar trend in the elastic modulii.
6. It is of great interest to compare the experimentally determined defect parameters with the theoretically estimated values based on Mott-Littleton type model calculation. Such extensive calculations are available for systems like alkali halides. In contrast, there has been only one such

calculation in KN_3 by Danemar[12] due to lack of data. To sharpen these calculations in KN_3 and extend the same to RbN_3, Prof. I. M. Boswarva of Imperal College, U. K. has undertaken the task using our data. He will try to calculate the defect parameters by using the "HADES" program of Harwell, a powerful technique recently developed to deal with non-cubic systems.

7. In addition, Dr. W. Mallard of Georgia State University is exploring the feasibility of using positron annihilation technique to study more details of the defect properties of the azide crystals grown by us.

8. Some other workers have studied this system by solid state techniques which have yielded many significant results. Of particular interest is the finding of Zakharov[15] and Royce[16] that the temperature dependence of the gaseous decomposition products of KN_3 at high temperature corresponds to the activation enthalpies for the ionic transport. Indeed this has led to Royce's conjecture that, at elevated temperature cations may arrive to the surface, form a potassium island on the surface by capturing free electrons and thus form the nucleus to initiate the decomposition process. Recent theoretical and experimental work of Williams[17] and Fair et al[18] has led to the understanding of the electronic states of azides and a very interesting possibility of the initiation of fast reactions by the injections of electrons and holes.

BIBLIOGRAPHY

1. A. D. Yoffe in Developments in Inorganic Nitrogen Chemistry (Elsevier, New York, 1966), p. 92.

2. Energetic Materials, edited by H. D. Fair and R. F. Walker, Vol. 1, (Plenum, New York, 1977).

3. A. L. Laskar, ARO-D Tech. Report no. CUP101 (1975).

4. G. Shirn, E. Wajda and H. Huntington, Acta Met. 1, 513 (1953),

5. W. J. Fredricks in Diffusion in Solids -- Recent Developments (Academic Press, New York, 1975), p. 381.

6. A. P. Batra and L. N. Slifkin, Phys. Rev. B12, 3473 (1975).

7. C. Bucci and R. Fiesehi, Phys. Rev. Letters, 12, 16 (1964).

8. E. G. Manning et. al., Rev. of Sc. Inst. 43, 324 (1972).

9. B. E. Taylor, Ph.D. Dissertation (1978), Clemson University.

10. E. Kitts, Ph.D. Dissertation (1973), University of N. Carolina at Chapel Hill.

11. R. W. Dreyfus and R. B. Laibowitz, Phys. Rev. 135, A1413 (1964).

12. A. Danemar, Ph.D. Dissertation (1972), Princeton University.

13. H. C. Abbink, Ph.D. Dissertation (1964), Iowa State University.

14. A. B. Lidiard in Handbuch der Physik, (Springer-Verlag, Berlin, 1957) vol. xx, p. 263.

15. A. Zakharov, Russian J. Phys. Chem. 45, 180 (1971).

16. B. S. H. Royce, A. D. Panafieu and T. J. Russel, Bull. Am. Phys. Soc. 19, 326 (1974).

17. F. E. Williams, in Chemical Dynamics, edited by J. O. Hirshfelder and D. Henderson (Wiley-Interscience, New York, 1971), p. 289-302.

18. H. D. Fair, et. al., Picatinny Arsenal Technical Report #4607 (1974).

JOURNAL DE PHYSIQUE *Colloque C7, supplément au n° 12, Tome 37, Décembre 1976, page C7-471*

IONIC DEFECTS AND THEIR TRANSPORT IN KN_3 AND RbN_3 (*) †

A. L. LASKAR (**), D. L. FOSTER and K. WAGNER

Department of Physics and Astronomy Clemson University, Clemson, SC 29631, U. S. A.

Résumé. — La conductivité et la diffusion des cations dans RbN_3 et KN_3 ont été étudiées. En ce qui concerne KN_3 l'enthalpie d'activation pour la formation de défauts est 1,60 eV, et celle pour la migration de défaut est 0,61 eV le long de l'axe *c* ; les valeurs correspondantes dans les plans de base sont 1,60 eV et 0,72 eV. L'enthalpie d'activation pour la diffusion du Na^+ dans KN_3 est 1,40 eV pour le transport de la masse le long de l'axe *c*. L'enthalpie d'activation RbN_3, pour la formation de défaut est 1,50 eV et celle pour la migration est 0,76. Les enthalpies d'activation pour la diffusion de Rb^+ dans RbN_3, parallèles et normales à l'axe *c* sont respectivement 1,43 and 1,45 eV. La diffusivité le long de l'axe *c* est trois fois supérieure à celle dans la direction normale. Ceci indique une grande différence dans la fréquence des *sauts* et/ou dans les notions d'entropies impliquées dans le processus de déplacement le long des deux directions. Dans les deux cas, RbN_3 et KN_3, il semble que la structure défectueuse est du type *Schottky* et que les cations sont les principaux transporteurs.

Abstract. — The electrical conductivity and the diffusion of cations in KN_3 and RbN_3 have been studied. For KN_3, the activation enthalpy for defect formation is 1.60 eV and that for the defect migration is 0.61 eV along the *c*-axis ; corresponding values in the basal planes are 1.60 eV and 0.72 eV. The activation enthalpy for the Na^+ diffusion in KN_3 is 1.40 eV for the mass transport along the *c*-axis. For RbN_3, activation enthalpy for defect formation is 1.50 eV. and that for the migration is 0.76 eV. The activation enthalpies for the diffusion of Rb^+ in RbN_3 parallel and normal to the *c*-axis are 1.43 and 1.45 eV respectively. The diffusivity along the *c*-axis is higher than that in the normal direction by a factor of three. This indicates large difference in the jump frequencies and/or entropy terms involved in the transport process along the two directions. For both RbN_3 and KN_3, it appears that the defect structure is *Schottky* type and the cations are the principal carriers.

1. **Introduction.** — The alkali azides are an interesting family of compounds known as *pseudo-halides* due to their strong ionic nature like alkali halides. They have a band gap of about 8 eV [1]. These materials undergo photo decomposition and thermal decomposition at high temperature but they do not lead to explosive deflagration as in some heavy metal azides.

Although the electronic and optical properties of azides have been extensively studied, there has been very little work with respect to the correlation of crystalline defects, their migration and interaction with the bulk properties presumably due to the nonavailability of large size single crystals. Reactions and rate processes in solids are often diffusion limited. Particularly the decomposition process in the alkali azides may be one of them [2]. So far, several studies of electrical conductivity in KN_3 have been reported [3-6]. Most of these studies were with powdered samples or pellets. The self-diffusion of potassium in KN_3 in the extrinsic range is also reported [7].

The present work was undertaken to grow and characterize large single crystals of KN_3 and RbN_3 and to investigate their bulk transport properties by the electrical conductivity and tracer diffusion experiments. Such studies could be used to help test and extend defect models developed for the simpler ionic solids to the more complex azide systems. Also the tetragonal lattice structure of the azides provides a unique opportunity to study the role of anisotropy on the ionic transport.

Many details of the experiments and results are given elsewhere [8] and are to be published. The main features of the results and their discussion are presented here.

2. **Experimental.** — Large single crystals used for this work were grown in the laboratory. KN_3 crystals were grown by Czchralsky technique and RbN_3 crystals were grown from solution by evaporation [9]. The starting material had about 50 ppm divalent impurities. The dislocation content of such crystals was found to be about $10^6/cm^2$ by counting the etch-pits.

(*) Work supported by AROD USA grant # DA-31-126-72-G-120 and DAH CO4-75-G-0130.

(†) Part of the material was also presented at the conference « La diffusion dans les milieux condensés ; théories et applications », June 22-25, 1976, at Saclay.

(**) Visiting Scientist at SRMP, C. E. N. de Saclay, France.

2.1 CONDUCTIVITY. — For the measurement of conductivity, samples were finely polished and subjected to annealing at 250 °C in 1 torr of nitrogen. For electrical contacts, both silver conductive paint and graphite were found satisfactory. The a. e. conductivity has been measured with the General Radio capacitance bridge assembly in the frequency range 1-10 kHz. The conductivity was measured in an interval of 5 or 10 °C and a waiting period of about an hour was allowed between measurements.

2.2 DIFFUSION. — The diffusion of cations in KN_3 and RbN_3 was studied by a tracer and serial sectioning technique. Few μCurie amount of the desired radioisotope is placed on the microtomed surface of a well-annealed sample. The sample is then diffusion annealed in nitrogen atmosphere for a stipulated time. Tracer diffusion work in these systems proved to be exacting. The azides are very light and brittle materials whereas the diffusivity of the cations is of the order of 10^{-12}-10^{-13} cm^2/s. A Jung rotary microtome was found satisfactory for 1 μm thick serial sectioning. Sample alignment within μm was achieved by using an optical lever arm of about 25 meters. A microelectrobalance with a precision of 0.1 μgm was used to weight the sections of having mass as low as 80 μgm.

3. **Results and discussion.** — 3.1 KN_3 : CONDUCTIVITY. — The general nature of the temperature dependence of the conductivity while electric field is applied normal the *c*-axis is represented in figure 1. In repeated cycling the Arrhenius plots during the cooling cycles were reproducible but not those during the heating cycles for some runs. This does not seem to be due to the electrodes but could be partly due to the absorption of moisture due to the hygroscopic nature of KN_3.

The extrinsic region for the conductivity seems to start at about 200 °C. From a series of runs, for the conductivity along the *c*-axis, the activation enthalpies for the intrinsic and extrinsic regions are found to be 1.4 eV and 0.61 eV respectively. For the direction normal to the *c*-axis the corresponding values are

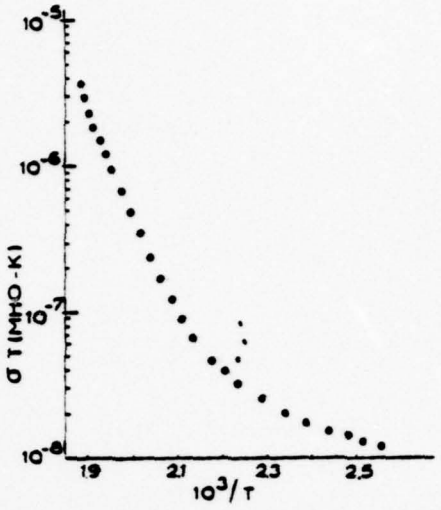

FIG. 1. — Arrhenius plot of conductivity in KN_3 with the applied field normal to the *c*-axis.

1.52 eV and 0.72 eV. These values are compared with the earlier results in the Table I. There is reasonable agreement between these results considering that some of the measurements were with powdered samples and pellets and without any preferred orientation. If the activation enthalpy in the extrinsic region is taken to be that for motion (H_m), then the formation enthalpy for the defects (H_f) can be estimated from the expression $H_f = 2(H - H_m)$. These values are listed also in Table I. The diffusion study of K^* in KN_3 [7] seem to establish that cations migrate via vacancies. Further, a reasonable correspondence between the experimentally obtained defect parameters and those from Danemar's [6] model calculation will indicate that the defect structure is Schottky type and the cations are the principal carriers.

It is noted that the anisotropy in the migration energy is about 0.1 eV. Using this value the anisotropy in the self diffusion of cations can be estimated from Mullen's numerical calculations [10]. However, this

TABLE I

Parameters for defect formation and migration in KN_3 (*activation enthalpies in* eV)

References	Type of samples and measurement	Orientation	H_f	H_m	$H = H_f/2 + H_m$
[3]	Pellet, D. C. conductivity		0.83	0.90	1.32
[4]	Pellet and solution grown D. C. conductivity		1.28	0.79	1.43
[5]	Same		1.25	0.76	1.38
[6]	Melt grown, A. C. conductivity	C 11	1.7	0.7	1.5
Present work	Melt grown, A. C. conductivity	C 11	1.60	0.61	1.41
Present work	Same	C ⊥	1.60	0.72	1.52

can be compared with the experimental value available only at one temperature [7]. At 590 K, the experimental value of D_A/D_C is 0.8. Using Mullen's prescription one estimates that $D_A/D_C = 0.5$, assuming that attempt frequency and entropy are same in both the directions. This will indicate that these two factors also have some anisotropy.

3.2 KN_3 : Na^* DIFFUSION. — The general nature of penetration profile for the Na^* diffusion in KN_3 is seen in figure 2. The upturn near the surface is pre-

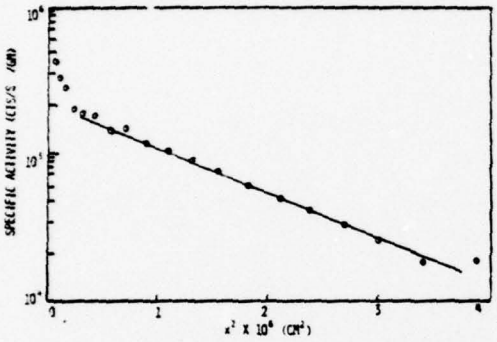

FIG. 2. — Penetration profile for Na^* diffusion in KN_3 at 286 °C.

sent in all the diffusion runs. Slight degradation of the surface and misaligned cuts may have caused this upturn at least in some cases. The usual correction for misalignment was applied. For some low temperature diffusion runs the linear segment of the penetration plot was followed by a tail due to the diffusion via short-circuit paths. Figure 3 represents the Arrhenius dependence of the diffusivities of sodium in potassium azide. At the highest temperature (298 °C),

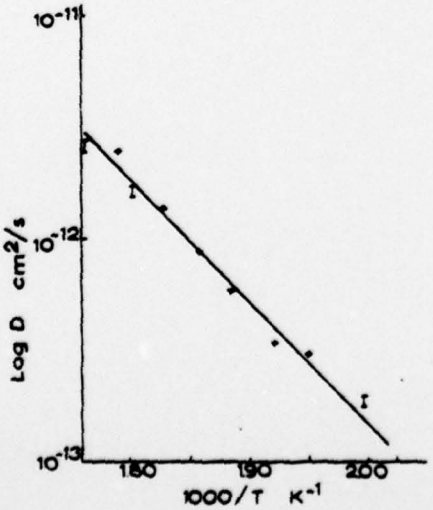

FIG. 3. — Diffusion of Na^* in KN_3 along the c-axis.

the uncertainty of the D value is high due to large misalignment and degradation of the surface. Omitting this datum, a least square analysis yields the following parameters :

$$D_0 = 11.5 \text{ cm}^2/\text{s} \text{ and } H = 1.40 \text{ eV}.$$

This is in very good agreement with the defect parameters determined from the conductivity experiments (table I). It is a further support that the cations are the principal charge and mass carriers in potassium azide and the defect structure is a Schottky type.

3.3 RbN_3 : CONDUCTIVITY. — The general nature of the temperature dependence of the conductivity in RbN_3 is seen in figure 4. The comments about the conductivity of KN_3 are applicable for RbN_3 also.

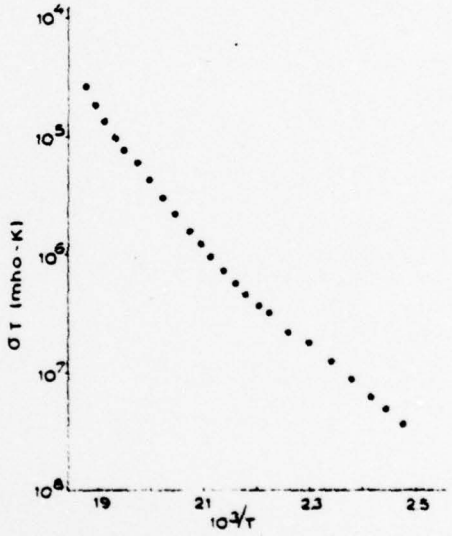

FIG. 4. — Arrhenius plot of conductivity in RbN_3 with the applied field parallel to the c-axis.

The intrinsic region of conductivity extends from about 210 °C-260 °C. From several such runs for the conductivity parallel to the c-axis the following activation enthalpies were estimated : 1.51 eV for the intrinsic range and 0.76 eV for the extrinsic range. If the latter value is taken as the enthalpy of motion (presumably for the cations, as will be supported by the diffusion results), then the formation enthalpy of the defects is estimated as 1.5 eV. A comparison of these numbers with Danemar's [6] values from a model calculation will indicate that the defect structure in RbN_3 is also Schottky type and the cations are the principal mobile charge carriers. Furthermore, an activation enthalpy of migration as high as 0.76 eV will correspond to the migration of cations by a vacancy mechanism.

The defect parameters could not be determined with certainty from the study of the conductivity in a direction normal to the *c*-axis. In some runs a *peak* was observed in the intrinsic range. The activation enthalpies in a direction normal to the *c*-axis were higher by 0.1-0.2 eV. and reproducibility was poor.

3.4 RbN_3 : Rb^* DIFFUSION. — The diffusion of Rb^* in RbN_3 has been measured both in the directions parallel and perpendicular to the *c*-axis in the temperature range 216-276 °C. Figure 5 represents the data. The narrow temperature range of this study is limited by the onset of decomposition at higher temperature and the termination of the intrinsic region below 200 °C due to the presence of impurities. The scatter in the data is appreciably more for the diffusivities measured normal to the *c*-axis. A possible reason may be the much smaller samples had to be used for the *c* direction due to the size of the grown crystals.

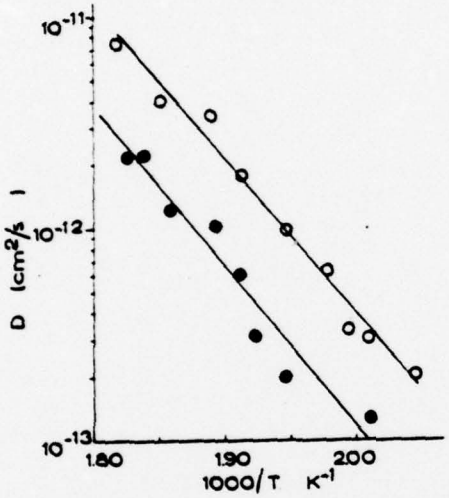

FIG. 5. — Diffusion of Rb^* in RbN_3. Open circles represent the diffusivities measured along the *c*-axis and the closed circles are for a direction normal to the *c*-axis.

A least square analysis yields the following diffusion parameters :

$$D_0^C (= D_{zz}) = 107 \text{ cm}^2/\text{s}, \quad H^C = 1.43 \text{ eV}$$

(Parallel to *c*-axis.)

$$D_0^A (= D_{xx}) = 52.3 \text{ cm}^2/\text{s}, \quad H^A = 1.45 \text{ eV}$$

(Normal to *c*-axis.)

Thus, the activation enthalpies for diffusion in both the directions are essentially same while the diffusivities along the direction parallel to the *c*-axis are higher than those normal to the *c*-axis by a factor of 3 for the temperature range studied. For the parallel direction, the activation enthalpy from the conductivity study is 1.51 eV and thus very close to the value obtained from the diffusion study. It supports the view that the cations are responsible for both change and mass transport.

3.5 RbN_3 : ANISOTROPY. — Alkali azides like KN_3 and RbN_3 have body-centered tatragonal lattice structure. In general, the defect parameters are expected to be different for directions parallel and perpendicular to the *c*-axis due to the anisotropic crystal structure. If the cations were the principal mobile species following a single mechanism, then the conductivity and diffusion results could be compared in a straightforward way. Since the conductivity results in the direction normal to the *c*-axis is less well defined, an attempt has been made to analyze the role of anisotropy from the diffusion data alone.

Mullen [10] has treated the anisotropic diffusion by vacancy mechanism for a tetragonal lattice. While the cations are moving along the basal plane by exchange lattice jumps with vacant lattice sites (ν_A) there is also a finite probability that the ions will also jump out of the basal plane in the *c*-direction with a jump frequency (ν_C). To deal with such coupled jumps he introduced correlation functions f_{AX} for the basal plane and f_{BZ} for the normal plane containing the *c*-axis. The diffusion coefficients are then given by

$$D_{zz} = \frac{1}{6} \nu_C \, nC^2 f_{BZ}$$

$$D_{xx} = \frac{1}{6} \nu_A \, nA^2 f_{AX} \qquad (1)$$

$$(C/A)^2 \, D_{xx}/D_{zz} = (\nu_A/\nu_C)\,(f_{AX}/f_{BZ}).$$

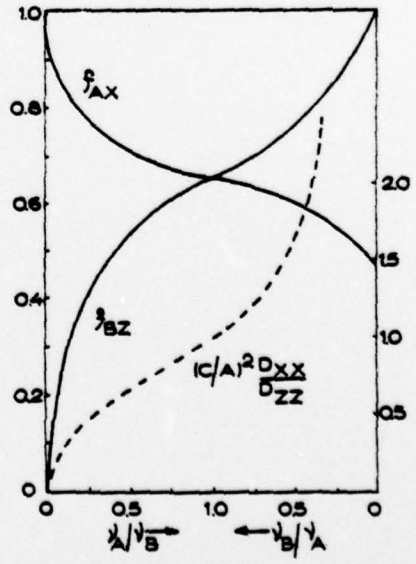

FIG. 6. — Anisotropy in the correlation functions and the diffusivities as a function of frequency ratio [10]. The scale to the left is to be used for the correlation functions.

where D_{ZZ}, ν_C and C stand for diffusivity, jump frequency and jump distance respectively along the c-axis ; D_{XX}, ν_A, and A are the corresponding symbols for a direction normal to the c-axis ; n stands for vacancy concentration. Figure 6 represents the graphical representation of Mullen's calculations for a 34×34 matrix. A later calculation of Danemar *et al.* [11] for a 7×7 matrix is essentially similar.

From the Arrhenius plots of figure 5, one determines $D_{ZZ}/D_{XX} \simeq 0.29$ at 250 °C (this ratio only changes slightly over the temperature range) leading to the following estimates from figure 6 ; $\nu_A/\nu_C = 0.05$, $f_{BZ} = 0.2$, $f_{AX} = 0.89$. Using the standard expression for ν [12] one obtains

$$\nu_A/\nu_C = \nu_0^A/\nu_0^C \exp[(S_m^A - S_m^C)/k] \times \exp[(H_m^C - H_m^A)/kT] \quad (2)$$

where ν_0 is the attempt frequency, S_m and H_m are the entropy and enthalpy of motion, k is the Boltzman constant and T is the absolute temperature. Superscript A and C refer to directions normal and parallel to the c-axis. It is interesting to note that the large ratio of ν_A/ν_C stems from the attempt frequencies and the entropy values in the two directions since there is only nominal difference in the activation enthalpies. There is no other experimental or theoretical results which could decide the major contribution to this ratio of ν_A/ν_C. It is more likely that the difference of entropy values along the two directions accounts for this large ratio.

Diffusion and conductivity results can be compared on the basis of Nernst-Einstein relation. Assuming that both charge and mass transport are caused by the cations migrating via vacancies, one obtains for a direction parallel to the c-axis : $D_{ZZ}/D_\sigma = 0.21$ (at 250 °C), $D_{ZZ}/D_\sigma = 0.22$ (at 230 °C). It is in excellent agreement with the corresponding correlation function $f_{BZ} = 0.2$. This indeed is a strong support to the earlier conjecture that cations are the principal mobile species in RbN_3.

In contrast, the corresponding values for the basal plane are

$D_{XX}/D_\sigma = 0.48$ (at 240 °C), $D_{YY}/D_\sigma = 0.71$ (at 224 °C).

These values are much smaller than the correlation function $f_{AX} = 0.89$ which indicates that some other mechanism is involved.

References

[1] Deb, S. K., *Trans. Faraday Soc.* **59** (1963) 1414.
[2] Panafieu, A., Ph. D. Thesis, Princeton University, 1974.
[3] Jacabs, P. W. M. and Tompkins, F. V., *J. Chem. Phys.* **23** (1955) 1445.
[4] Maycock, J. N. and Pai Verneker, V. R., *J. Appl. Phys.* **40** (1969) 5015.
[5] Maycock, J. N., Pai Verneker, V. R. and Gorzynski, C. S. Jr., *Phys. Status Solidi* **37** (1970) 857.
[6] Danemar, A., Ph. D. Thesis, Princeton University, 1972.
[7] Sharma, J. and Laskar, A. L., *J. Phys. & Chem. Solids* **34** (1973) 989.
[8] Foster, D. L., Wagner, K. and Laskar, A. L., ARO-D Technical Report No. CUP 101 (1975) ; Wagner, K., M. S. Thesis (1975) and Foster, D. L., Ph. D. Thesis (1976) Clemson University.
[9] Foster, D. L., Wagner, K. and Laskar, A. L., *J. Crystal Growth* **32** (1976) 33.
[10] Mullen, J. G., *Phys. Rev.* **124** (1961) 1723.
[11] Danemar, A., Welch, D. O. and Royce, B. S. H., *Phys. Status Solidi* (b) **55** (1973) 201.
[12] Girifalco, L. A., *Atomic Migration in Crystals* (Blaisdell, New York) 1964, p. 92.

DISCUSSION

R. J. Friauf. — For conductivity in potassium azode you showed an extrinsic region at lower temperatures and an intrinsic region at higher temperatures. But for diffusion of sodium your results showed just one line on the Arrhenius plot, with no break at the lower temperatures for the extrinsic region. This seems peculiar. If additional vacancies are introduced by impurities, they should influence diffusion as well as conductivity.

A. L. Laskar. — The temperature range covered by the Arrhenius plot for Na^+ diffusion in KN_3 really falls within the intrinsic range seen in the study of conductivity of KN_3. Lowest temperature point for the diffusion experiment come close to the extrinsic range, and may be a reason for the higher value of D with respect to the single Arrhenius line. This is discussed in the text of the paper.